Non-classical autophagy activation pathways are essential for production of infectious Influenza A virus *in vitro*

Tisza A.S. Bell[1], Nileena Velappan[1], Cheryl D. Gleasner[1], Gang Xie[1], Shawn R. Starkenburg[1], Geoffrey Waldo[1], Shounak Banerjee[1] and Sofiya N. Micheva-Viteva[1*]

[1] Bioscience Division, Los Alamos National Laboratory, Los Alamos, New Mexico, USA

***Correspondence: sviteva@lanl.gov**

Abstract

Autophagy is a critical mechanism deployed by eukaryotic cells in response to stress, including viral infection, to boost the innate antimicrobial responses. However, an increasing number of pathogens hijack the autophagic machinery to facilitate their own replication. Influenza A virus (IAV), responsible for several global pandemics, has an intricate dependence on autophagy for successful replication in mammalian cells. To elucidate key chokepoints in the host stress responses facilitating IAV replication, we constructed a meta-transcriptome of IAV and host gene expression dynamics during early (1-3 hpi), mid (4-6 hpi) and late (8-12 hpi) stages of the viral replication cycle at two multiplicities of infection (MOI): 1 and 5. We supplemented the global transcriptome study with phosphoproteomic analysis of stress-activated protein kinase (SAPK/JNK) signaling in lung carcinoma (predominantly used as an *in vitro* model of IAV replication) and normal human bronchial epithelial cells. We report significant differences in the activation profiles of autophagy regulating genes upon IAV infection at the two MOI as well as divergent dependence on ULK1 signaling within the normal and cancer cells. Regardless of the cell model, JNK-Thr187 signaling was crucial for the production of infectious viral particles.

Keywords: Influenza A virus; meta-transcriptome; RNA-seq; autophagy; mechanistic target of rapamycin complex 1 (mTORC1); ULK1 signaling; stress-activated protein kinase (SAPK/JNK); infectious particles

Take Aways

- Inhibition of ULK1 function does not change the course of autophagy activation in non-starved, Influenza A infected lung epithelial cells.
- IAV replication simultaneously activated transcription of key genes regulating mTORC1 and autophagy in human lung epithelial cells.
- Influenza A virus co-opts host stress response mechanisms regulated by the c-jun N-terminal kinase to boost production of infectious virus particles.

1. INTRODUCTION

Autophagy is a pro-survival mechanism supporting eukaryotic cell adaptation to various environmental stressors, such as nutrient starvation, UV irradiation, and microbial infections [1-5]. The current concepts in cellular biology attribute plurality of functions to autophagy, including sustenance of healthy cellular physiology and energy homeostasis; regulation of inflammation; and support of innate and adaptive immunity through pathogen clearance and antigen presentation [6-14]. While the cell signaling pathways regulating autophagy initiation are stress factor specific, the core mechanism of autophagosome biogenesis invariably leads to the formation of double-membraned vesicles that randomly or selectively engulf cytoplasmic cargo. For the degradation of the captured cargo, autophagosomes fuse with lysosomes forming autolysosomes where low pH and abundance of proteolytic enzymes aid the recycling of damaged organelles into anabolic building blocks and energy source molecules. Additionally, microbes engulfed by the eukaryotic cells via endocytosis are targeted to the autolysosomes for degradation [15, 16].

The role of autophagy as an intrinsic mechanism of eukaryotic cell resistance to pathogens has sparked interest in host-directed therapeutics development [7, 17]. Due to the great diversity

of DNA and RNA virus replication mechanisms, development of broad-spectrum antiviral therapeutics remains an impossible task. To address this problem, anti-viral treatment protocols based on augmentation of host cell antimicrobial mechanisms, such as autophagy, can be implemented [18-20]. Paradoxically, a growing list of viruses and intracellular bacteria take advantage of host autophagic machinery to promote their own replication [10, 21-23]. To further complicate the issue, in discrete cases autophagy activation has both pro- and anti-viral function [18, 24]. Therefore, identification of pharmacological targets for broad-spectrum antiviral therapeutics demands in depth understanding of the autophagic machinery components that enhance host defenses and those co-opted for virus replication.

Influenza A virus (IAV) is an enveloped respiratory pathogen causing seasonal infections with morbidity and mortality among human and animal populations. Historically, influenza viruses have been responsible for several devastating global pandemics [25, 26]. Periodic cycling of influenza subtypes and strains requires the design of seasonal vaccines that often miss unexpected rearrangements of viral antigens [27]. IAVs evolve resistance to antiviral drugs and genomic re-assortment events further accelerate the global dissemination of resistant viruses [28, 29].

When traditional anti-viral treatments fail, therapeutics against host regulatory proteins may come to the rescue. It has been previously shown that chemical inhibition of autophagy improved the survival rate of the H5N1-infected host by reducing inflammation and severe lung damage [30]. Notwithstanding the evidence, the relationship between IAV and autophagy is quite complicated. The autophagy machinery was found to facilitate influenza virus replication, while at the same time most IAV strains hijack host translational machinery by activating the mechanistic target of rapamycin (mTOR) complex 1 to ensure viral protein synthesis [31-33]. The IAV dependence on both mTORC1 and autophagy is seemingly paradoxical because activation of

mTORC1 through phosphoinositide 3-kinase (PI3K) and AKT signaling results in mTORC1-directed phosphorylation and inhibition of autophagy activation kinase 1 (ULK1) complex [34-37].

The IAV causing seasonal epidemics in humans (strains H1N1 and H3N2) utilize their non-structural protein 1 (NS1) as an anti-apoptotic agent via direct interaction with the p85β subunit of PI3K and activation of AKT1 signaling pathway [41-43]. Thus, the viral NS1 stimulates mTORC1 kinase function to facilitate protein synthesis and cap-dependent translation initiation through cascade of phosphorylation events, including p70 S6 kinase and 4E-BP1 [31, 38]. Activated mTORC1 is supposed to inhibit autophagy through ULK1 signaling, however it supports the synthesis of viral proteins acting as autophagy stimulation factors, including hemagglutinin (HA) and ion channel matrix 2 (M2) [33]. Specifically, the influenza virus M2 protein interaction with the Microtubule-associated protein light chain 3 (LC3), a core structural protein of the autophagosomes, was found to inhibit autolysosome formation while redirecting the LC3-M2 complex to the plasma membranes [33, 44]. This process is associated with delays in apoptosis initiation and facilitation of virion assembly and budding [44, 45].

Current models describe autophagy as a host response mechanism activated during the late stage of IAV replication [45], while mTORC1 and mTORC2 activation by IAV infection was reported to occur midway through the IAV replication cycle [31]. These models, based on Western blot (WB) phosphoproteomic data analysis, are influenced by two main experimental shortcomings: sensitivity limitations of WB and use of cancer cells as host models for *in vitro* IAV infection studies. Here, we sought to elucidate the autophagy-regulating component that is essential for IAV replication in lung epithelial cells. We applied a highly sensitive analytical approach and validated our findings in a non-cancer cell model. We performed a RNA-sequencing

94 based meta-transcriptomic study of IAV and host gene activation dynamics throughout the virus
95 replication cycle at two multiplicities of infection (MOI), 1 and 5. We found that viral load has a
96 strong influence on the mode and dynamics of host cell protective responses and autophagy
97 activation. With a protocol that does not induce autophagy due to serum starvation of the host cells
98 during the virus absorption stage, we detected simultaneous activation of mTOR complex 1 genes
99 and key autophagy regulating genes early upon virus infection (1-3 hpi at MOI 1). Subsequent
100 phosphoproteomic analysis verified that the classical autophagy activation pathway through ULK1
101 signaling did not play a significant role in the autophagy activation upon IAV infection, while the
102 activation of c-jun N-terminal kinase (JNK) was essential for viral protein accumulation. JNK, a
103 stress-activated protein kinase (SAPK) activated by various viruses [46-48], is stimulated by direct
104 interaction with the IAV NS1 protein [49]. We show that chemical inhibition of JNK abrogated
105 viral protein accumulation in lung carcinoma A549 cells and significantly inhibited infectious viral
106 titer in non-cancer cells. Host-directed antiviral therapy targeting key regulators of non-classical
107 autophagy pathways, such as JNK/SAP, could show less toxicity *in vivo* compared to a
108 pharmacological inhibition of the classical autophagy pathways that are essential for proper host
109 immune defenses.

110 **2. RESULTS**

111 *2.1. Serum depletion activates autophagy prior to Influenza A virus replication in vitro*

112 Cleavage of IAV hemagglutinin (HA) is required for fusion of the viral capsid with host-cell
113 endosomal membranes. Proteases secreted by the respiratory epithelium are responsible for HA
114 cleavage *in vivo* IAV infection [58-60]. The majority of *in vitro* cell models (MDCK, HEK293, or
115 A549) utilized to study the role of autophagy in IAV replication do not produce proteases that

cleave HA necessitating the addition of trypsin to promote virus infectivity. Typically, during the one-hour virus absorption stage, the host cells are incubated in serum free media containing the infectious virus and TPCK-trypsin [31, 33, 44, 45, 61]. Applying time-lapse microscopy, we monitored the cellular localization of transcription factor EB (TFEB) in live cells, as a biomarker of autophagy activation [62], and registered TFEB translocation into the nucleus of mock-treated A549 cells within 40 minutes of incubation in serum and virus free media (S1-A). Consistent with TFEB nuclear localization, we observed a significant drop in the levels of phosphorylated ribosomal protein S6 kinase β-1 (p70S6K1) indicating inhibition of mTORC1 activity (S1-B). Thus, serum depravation protocols for *in vitro* infection of cancer cell lines with IAV generate data that is biased to a condition where mTORC1 function is downregulated and autophagy is induced prior to the initiation of viral replication. To investigate the role of IAV infection on autophagy activation, we adapted a protocol that did not include a serum starvation step. With this protocol, we were able to study the normal course of autophagy activation upon IAV infection (S1-C) and found that H3N2 strain, *A/Port Chalmers/1/73*, showed higher tropism to A549 cells compared to the H1N1 strain, *A/PR/8/1934* (S1-D). Therefore, in this study we used the H3N2 strain to investigate the role of autophagy in IAV replication in lung epithelial cells.

2.2. Autophagy activation correlates with Influenza virus A load

Employing strand-specific RNA-sequencing (RNA-seq) of infected A549 cells, we simultaneously measured the kinetics of A/PCh/1/73 replication and the expression of host genes affected by IAV replication at 1, 3, 4, 6, 8, and 12 hours post infection (hpi). In order to measure virus replication, we generated RNA-based growth curves by normalizing the total virus reads to the total host read coverage (Fig.1A). The viral RNA accumulation profile was consistent with the virus titration growth curves (S1-D). To reproducibly detect reads from genes with low

transcription rates, we performed infections with moderate (1) and high (5) multiplicities of infection (MOI) representing the ratios of host cells to infectious virus particles. At MOI5, we observed a rapid increase in the viral transcript levels that accounted for 10% of the total RNA reads within 2 hours of infection and plateaued between 4 and 8 hpi, accounting for 75% of the total RNA reads (Fig.1A). In contrast, we observed exponential viral growth within 4 hours of infection at MOI1. By 12 hpi, viral RNA levels started to decline in both infection conditions.

The objective of our study was to evaluate the effect of IAV replication on the expression profiles of genes involved in the regulation of autophagy, mTOR signaling pathways, and innate immunity. We observed greater dynamics in global host transcriptome (with DGE $\geq$ 2-fold change) during early stages of IAV infection compared to later timepoints of virus replication when data was normalized to time-matched mock-treated cells (Fig.1-2). Virus load played a significant role in the gene expression dynamics.

At a moderate virus load (MOI1), within 4 hours of infection, we observed a sequential activation of genes that regulate the early stages of the autophagy pathway (Fig.1B). We witnessed initiation of autophagy elongation phase by the activation of ULK2 and Autophagy and Beclin-1 Regulator protein (AMBRA1) (1 hpi) followed by ATG13 and RUBCN (3 hpi) transcript accumulation. Activation of ATG7 and ATG10 gene expression corresponds to the elongation of nascent autophagosomal membrane at 1 hpi. ATG4A, a regulator of the final stage of functional autophagosome formation (phagophore membrane fusion), was differentially upregulated at 6 hpi, while the MAPK1LC3 gene activity, facilitating the phagophore membrane fusion, remained unchanged up to 12 hpi.

During the period of exponential virus replication (1 to 4 hpi), we observed a gradual accumulation of the AMBRA1 transcripts encoding for a core subunit of the PI3K complex that is

essential for the initiation and maturation of autophagosomes. AMBRA1 gene expression declined at later stages of infection (6-12 hpi) when the viral load surpassed 50% of total RNA reads, overwhelming the host transcription machinery.

The gene activation dynamics of autophagy regulators showed oscillatory pattern at high virus load (MOI5). Compared to DGE in cells infected with lower MOI, at MOI 5 gene expression of AMBRA1, ULK2, ATG10, and ATG16L, spiked 3 hpi instead of 1 hpi. We could not detect ATG13 activation in the samples infected with IAV at MOI5, while this key regulator of the autophagy initiation was differentially activated for five hours (3-8 hpi) in A549 cells infected at MOI1. It is possible that DGE dynamics could have been accelerated at high virus load (MOI5), and therefore, we were only able to detect the "tail" of the gene activation burst at 1 hpi for genes regulating the early stages of autophagosome formation: ATG5, ATG16L1, ATG3 (Fig. 1B). The observed delay of ATG10 activation at MOI5 (3-4 hpi) compared to infection at MOI1 (1-3 hpi) may be indicative of a secondary oscillatory burst in the activation of autophagy gene regulators due to increased virus burden.

A steady accumulation of BAD gene transcripts was characteristic of the A549 cells infected at MOI5 (Fig.1B). BAD protein positively regulates apoptosis by forming dimers with cell death-reversing BCL-2 protein. Consequently, the transcript levels of BCL2L1 were upregulated within 1 hour of infection at MOI5. Another DGE profile specific to lung carcinoma cells infected with high IAV load was the upregulation of RPS6KB2, a mTOR substrate responsible for stimulation of protein synthesis through phosphorylation of S6 ribosomal protein and eukaryotic translation initiation factor 4B (eIF4B). In contrast, RPS6KB2 was not differentially expressed in A549 cells infected at MOI1, while the transcript levels of global protein synthesis inhibitor, EIF2AK3, increased between 4 and 6 hpi. The cause for EIF2AK3 gene activation could be energy depletion

185 in the lung cells hosting rapidly replicating virus. Interestingly, EIF2AK3 gene transcription
186 exceeded background levels within the first 3 hours of infection at a high viral load. These data
187 suggest that host cells attempted to counteract viral replication by shutting down protein synthesis,
188 while virus co-opted host cell protein synthesis machinery for replication (Fig.1B).

189 MAPK3/ERK controls various biological functions, including cell growth, survival, and
190 differentiation. Depending on interaction with a pathway-specific substrate, MAPK3 can activate
191 translation through EIF4EBP1 and apoptosis through phosphorylation of BAD. Additionally,
192 MAPK3 activates mTORC1 by phosphorylation of RAPTOR and TSC complex [63, 64].
193 Activated mTORC1 positively regulates protein synthesis and inhibits activation of autophagy
194 pathway through ULK1/2 complex. Surprisingly, MAPK3 and autophagy regulating genes were
195 simultaneously activated during the exponential phase of IAV replication (Fig.1B, MOI1). At
196 higher MOI (5), MAPK3 gene expression spiked at 3 hpi and returned to base levels thereafter.
197 These results suggest that cell stress induced by the high burden of viral protein synthesis could
198 initiate negative feedback mechanisms to activate MAP3K transcription.

199 Collectively, our unbiased transcriptome study of lung cancer cells infected with IAV
200 demonstrated that the autophagy pathway was activated during the exponential stage of virus
201 replication. High virus load (MOI5) stimulated both pro-apoptotic gene groups (BAD and
202 BCL2L1) and genes essential for enhanced protein synthesis (RPS6KB2) within an hour of
203 infection. At MOI1, genes regulating initiation of autophagy were activated during the exponential
204 phase of IAV replication. Autophagy gene expression showed oscillatory behavior both at high
205 (MOI5) and low (MOI1) virus load.

206 *2.3. IAV replication simultaneously activated genes regulating mTORC1 and ULK1 pathways*

mTOR regulatory complex is activated at nutrient rich environment to positively regulate protein synthesis, cell growth and differentiation. A common set of protein kinase regulatory proteins associate with the proteins Raptor and Rictor to form two complexes: mTORC1 and mTORC2 respectively, each complex carrying a distinct function. Activation of mTOR1 facilitates protein synthesis through phosphorylation of ribosomal protein kinase S6K (RPS6K), while mTORC2 regulates cytoskeleton dynamics and cell survival [35, 36]. To promote cell survival, mTORC2 phosphorylates and activates SGK1 and AKT kinases. Growth factors activate mTORC1 through the phosphoinositide-3 kinase (PI3K)-AKT or SOS-MAPK3/ERK signaling axis [65, 66]. Additionally, the LRP-GSK axis neutralizes the inhibitory action of the TSC1/2 complex and positively regulates mTORC1 activity [67].

Previous studies have shown that H1N1 IAV ramps up the production of viral proteins through direct activation of PI3K [31, 33]. Here, we observed transcription activation of PI3K catalytic subunit alpha (PI3KCA) within an hour of H3N2 IAV infection at MOI1. Thereafter, PI3KCA transcript levels gradually decreased during the exponential accumulation of viral RNA to spike again at 12 hpi (Fig.2A, MOI1). In contrast, we detected no activation of PI3KCA gene expression upon infection with high MOI. (Fig.2A, MOI5) Similarly, gene transcription of Raptor (RPTOR) and its activator AKT1 was stimulated early upon IAV infection at MOI1 and was inhibited at later stage of the virus replication cycle (Fig.2, MOI1). Both genes were slightly activated within an hour of IAV infection at high virus load (Fig.1A and 2, MOI5).

Interestingly, the AKT isoforms were activated upon IAV infection in a sequential order: AKT1 at 3-4 hpi, AKT2 at 4-8 hpi with maximum expression levels at 6 hpi, and AKT3 at 3-8 hpi (Fig.2, MOI1). At high virus load, the AKT3 levels peaked at 6 hpi (Fig.2, MOI5). AKT kinases regulate many processes including cell metabolism and survival via mTOR dependent and

independent signaling pathways. The timing of AKT1/2/3 isoform, RPTOR, and RICTOR gene activation suggested that AKT1 and AKT2 regulate protein synthesis through mTORC1 signaling, while AKT3 gene function can be linked to cell survival through mTORC2 activation. Exponential IAV growth coincided with activation of RICTOR gene transcription (Fig.1A and Fig.2, MOI1). RICTOR gene activation followed oscillatory pattern similar to DGE of the major autophagy regulators both at lower and high virus load. In comparison, SOS1 and SGK1 genes regulating cell survival and stress responses were upregulated only at the early stages of virus replication (Fig.2).

The ULK1 gene was upregulated upon IAV infection at MOI 1 and sustained transcription activity until the later stage of viral replication (12 hpi). In contrast, at high virus infection load (MOI5) we observed a less pronounced ULK1 upregulation at 3 hpi followed by gene inhibition at later stages of virus replication (Fig.2, MOI5). Notably, ULK2 gene transcription was inhibited in host cells infected with the lower viral load (MOI1). In contrast, ULK2 gene was activated at the early stage (3 hpi) of IAV infection at MOI5. The ULK2 expression profile was consistent with that of AMPK subunit alpha (PRKAA1) and showed inverse DGE pattern to the ULK1 gene expression (Fig.2). In summary, our transcriptome data indicate that upon IAV infection at MOI1 nutrient depletion may not contribute to the stimulation of the autophagy pathway.

Collectively, we observed steady accumulation of ULK1, MAPK3/ERK (Fig.1B, MOI1) and LRP6 (Fig.2, MOI1) gene transcripts throughout the virus replication cycle indicating that genes regulating autophagy and mTORC1 activation were simultaneously activated. The oscillatory pattern of key autophagy (ATG7, Fig.1B, MOI1) and mTORC2 (RICTOR, Fig2, MOI1) gene expression profiles suggests that viral replication activates two major cell survival pathways: autophagy and mTORC2.

2.4. IAV replication activates autophagy in lung epithelium cells independently of the ULK1 signaling pathway

Our global transcriptome analysis revealed previously uncharacterized correlation between IAV load and activation of ULK gene transcription. While ULK1 gene was consistently transcribed in A549 cells throughout the IAV virus replication cycle at MOI1, its expression dynamics remained mostly unchanged at MOI5 (Fig.2, S2). Therefore, we further investigated on a post-transcriptional level the role ULK1 plays in autophagy activation and IAV replication.

Applying Western blot (WB) analysis, we could barely detect viral protein accumulation 12 hpi at MOI1 (S3), while the transcriptome analysis showed that viral RNA had reached maximum levels at 4 h post-infection (Fig.1A). We could detect accumulation of viral proteins (M2 and NP) with WB as early as 6 hpi at MOI5 (Fig.3A). At this high virus load, total IAV transcript levels reached their maximum levels between 3 and 4 hpi and declined at 6 hpi (Fig.1). The observed time gap between transcript and protein accumulation is largely due to the substantial difference in target detection sensitivity between the two analytical methods. Quantitative analysis of percentage infected cells via flow cytometry indicated that at MOI1 close to 10% of the total cell population harbored the virus, while at MOI5 half of the population become infected (S3). Since both methods analyze bulk transcript or protein levels, the WB data could only reveal the biomarkers with the most prominent changes elicited by IAV infection.

Regardless of WB sensitivity limitations, we could observe activation of autophagy through accumulation of lipidated LC3B-II form of the microtubule-associated protein light chain protein that coincided with IAV protein accumulation (Fig.1A) [16]. When autophagy is activated via the classical pathway, the levels of ULK1 phosphorylation at Ser757 subside due to inhibition of mTORC1 activity [2]. Since the global transcriptome analysis showed continuous activation of

ULK1 gene expression at MOI1 and no significant changes in gene activity at MOI5, we further investigated the role of ULK1 in infected cells enduring metabolic stress due to high virus protein levels at MOI5. Inhibition of ULK1 phosphorylation at S757 with small molecule SBI0206965 did not change the course of autophagy activation upon IAV infection as we observed continuous accumulation of lipidated LC3-II form in virus-infected cells (Fig.3A-B). At the same time, we observed no reduction of viral protein levels in A549 cells treated with the ULK1 inhibitor (Fig.3A).

We further validated our WB results by applying immunocytofluorescence with anti-LC3B antibodies. We observed autophagosome vesicle formations in IAV-infected A549 cells when ULK1 signaling was inhibited with a small molecule (S4 and Fig.3C) thus confirming the WB-based proteome data. Collectively our data indicated that autophagy was activated through an alternative to ULK1 signaling pathway during IAV infection.

2.5. IAV infection upregulates AKT and Stress Response Kinase JNK activity in A549 cells midway through the virus replication cycle

Previous *in vitro* studies of IAV infection have demonstrated that viral proteins stimulate mTORC1 activity to ensure virus protein expression and promote successful replication [33, 41]. Additionally, mTORC2 function supports host survival in the later stages of IAV replication when cells undergo significant stress [31].

To validate our findings from the global transcriptome analysis of mTOR-regulatory complex differential gene expression , we measured mTORC1 and mTORC2 activity in IAV infected A549 cells. We observed that at MOI1 the phosphorylation levels of p70 S6 kinase 1 (S6K), a mTORC1 substrate, remained unchanged, while AKT1- Ser473 phosphorylation, a mTORC2 substrate, increased throughout the virus replication cycle (Fig.4A). Notably, the exponential increase in

298 phosphorylated AKT-Ser473, an indicator of cell stress, coincided with the accumulation of viral
299 transcripts (Fig.1A). Our results also demonstrated that the Thre389 phosphorylation on the S6K
300 increased proportionally to the virus load at the later stage of virus replication (Fig. 4B).
301 The phosphoproteomic data presented here demonstrated that pro-survival mechanisms
302 dependent on AKT-Ser473 phosphorylation were activated at mid throughout the late stage of the
303 virus replication cycle, while mTORC1 activity was not affected in cells infected with IAV at
304 MOI1. We detected mTORC1 activation in the later stages of IAV replication specifically at very
305 high MOI, when mTORC1 function was required to satiate the high demand for protein synthesis
306 (Fig. 4B: 9 hpi vs 6 hpi).
307 Together with the activation of AKT anti-apoptotic signaling, we investigated the JNK stress-
308 response regulator upon virus infection. JNK activation is a common response to many stress
309 stimuli, including endoplasmic reticulum (ER) excessive stress, causing apoptotic cell death
310 through regulation of the BCL2 family proteins [68-70]. Our Western blot results showed
311 consistent accumulation of Thr183-phosphorylated JNK in IAV infected cells. This was
312 proportional to the synthesis of viral proteins (Fig.4C). Activation of JNK signaling occurred
313 midway through the IAV (H3N2) replication cycle and coincided with the AKT-pSer473 anti-
314 apoptotic signaling (Fig.4A and C). For comparison, we detected accumulation of phosphorylated
315 JNK-Thr185 at later time upon infection with similar MOI of IAV (H1N1) subtype (S3C). These
316 findings underline strong correlation between the accumulation of high virus protein amount and
317 stress-activated JNK signaling. Importantly, pharmacological inhibition of JNK signaling through
318 Thr183 phosphorylation resulted in a significant decrease in IAV protein synthesis and a weaker
319 autophagy pathway stimulation, measured as reduced levels of the lipidated LC3B-II (Fig.4D). We
320 observed that the LC3-II/LC3-I ratio increased 8-fold within 12h of virus infection compared to

the time matched mock-treated A549 cells with functional JNK signaling and only 2-fold in the IAV infected cells exposed to JNK inhibitor (Fig.4D).

Taken together, the phosphoproteomic analysis of AKT-Ser473 and JNK-Thr187 signaling upon infection of A549 cells with IAV indicate that viral proteins stimulated host anti-apoptotic adaptations through activation of AKT and JNK stress response mechanisms. Pharmacological inhibition of JNK signaling dramatically reduced viral protein synthesis in IAV-infected lung carcinoma A549 cells.

2.6. Pharmacological inhibition of JNK-Thr187 signaling decreased IAV titer in normal human bronchial epithelial cells (NHBE) in vitro

Since the cancer cells, including the A549 line, used as models to study IAV replication may regulate stress response and survival mechanisms differently compared to normal human lung cells, we further investigated the role of JNK signaling in normal human bronchial epithelial (NHBE) cells *in vitro* infected with the H3N2 *A/PCh/1/73* strain.

Western blot analysis of total protein extracted from mock-treated and IAV-infected NHBE cells showed different responses to ULK1 and JNK signaling inhibition compared to the A549 cancer cell line. The NHBEC were more sensitive to the small molecule compounds SBI0206965 and SP600125 targeting ULK1 and JNK signaling, respectively, therefore we applied lower drug concentrations. Unexpectedly, ULK1 inhibition caused a decline of JNK-T183 phosphorylation in IAV-infected NHBEC, although the viral protein (M2) accumulation and activation of LC3B synthesis remained unaffected (Fig.5A). In contrast to the A549 cancer cells, we detected LC3B accumulation only in IAV infected NHBEC, either untreated or treated with SBI0206965 to inhibit ULK1 signaling. LC3B in NHBEC treated with the JNK inhibitor SP600125 was barely detectable even in IAV-infected populations (Fig.5A). Immunofluorescence analysis, a more sensitive

protein detection method, showed that IAV-infected NHBEC produced LC3B. Furthermore, the percentage of NHBEC harboring IAV protein dropped significantly upon pharmacological inhibition of JNK signaling (Fig.5B) indicating at its significance for the IAV (H3N2) replication.

We further validated the role of JNK and ULK1 signaling in IAV replication analyzing the infectious virus titers generated by NHBE, adenovirus transformed NHBE (BEAS-2B), and lung epithelium carcinoma cell line (A549). We found that NHBE from three genetically unrelated healthy donors produced infectious virus titers comparable to those released by the immortalized cell lines. Pharmacological inhibition of JNK function reduced the levels of infectious IAV particles by two-fold in the transformed cell lines and by 20-fold in the NHBE cells (Fig.5C). These results complemented our Western blot and immunocytochemistry studies and demonstrated that JNK-signaling inhibition in NHBEC has stronger effect on IAV replication compared to cell models based on immortalized cell lines.

Collectively, our data indicated that IAV (H3N2) activates autophagy independently of the classical ULK1 signaling pathway in normal and cancer (A549) lung epithelial cells. Although, IAV infection universally activated JNK signaling in all tested cell models, the immortalized cell lines were less dependent on this regulatory response for production of infectious virus compared to NHBEC. The JNK-Thr187 signaling appeared as a stress regulatory mechanism activated by the rampant synthesis of viral proteins. Therefore, inhibition of JNK-Thr187 signaling decreased the host cell capacity as a virus "factory" and resulted in a significant reduction of infectious IAV titer *in vitro*.

2.7. IAV matrix protein M2 interaction with the host LC3B protein activates autophagosome formation

Our Western blot results have consistently indicated that IAV infection activates autophagy in strict correlation to accumulation of viral proteins (Fig.3A, 4D, and 5A). Since detection of the lipidated LC3B-II form was contingent to high viral protein load, we designed experiments to test whether direct interaction between the viral M2 protein and the autophagosome core protein occurs *in situ* and activates autophagy independently of the classical (ULK1) or alternative (JNK) signaling cascades. Previous studies have inferred interaction between the two proteins from *in vitro* binding studies and infections with M2-deficient H1N1 virus [44]. Here, we utilized split green fluorescent protein (GFP) methodology [55] to directly test M2-LC3 interaction in live cells. We tagged each LC3B and M2 proteins with GFP fragments 10 (G10) and 11 (G11). Plasmids expressing proteins tagged with the GFP fragments were co-transfected in HEK293T cells. No fluorescence was detected in transfected cells prior to addition of the GFP1-9 scaffold domain (data not shown). Since the GFP1-9 utilized in this study was not optimized to fold properly in mammalian cells, we supplied purified and folded GFP1-9 peptide *in trans* similar to the antibody staining techniques. Thus, we registered protein-protein interactions that occurred in live cells in fixed cells supplemented with the GFP1-9 scaffold.

Guided by previous knowledge that M2 forms homo-dimer and tetramer complexes [71], we co-transfected plasmids expressing M2 protein tagged with G10 and G11 as a positive control for our assay. As expected, complementation of the split-GFP fragments in HEK293T cells expressing M2-tagged proteins resulted in fluorescence that highlighted the extracellular membrane and intracellular membranous structures where M2 resides (Fig.6A, upper left panel). Self-oligomerization of LC3B protein has not been previously reported, therefore we applied G10 and G11-tagged at the N-terminus of LC3B-expresing plasmids as a negative control. Unexpectedly, split-GFP complementation of the LC3B-tagged proteins recovered the GFP fluorescence activity

(Fig.6A, upper right panel). The fluorescent signal was consistent with that of native LC3B-I protein cellular localization (S4). Finally, co-transfection of plasmids expressing tagged LC3B and M2 proteins produced fluorescently labeled cell membrane and phagosomes consistent with the localization of LC3B-II and M2 (Fig. 6A, lower panel).

We further validated the effect of M2 accumulation on LC3B lipidation required for inclusion into cellular membranes. Applying Western blot analysis, we compared the levels of lipidated LC3B-II in HEK293T parental cell line and a derivative cell line with stable chromosomal integration of M2 gene under Tet-inducible promoter, HEK293-M2 [56]. Activation of M2 gene expression upon addition of tetracycline resulted in higher M2 protein levels and increased the accumulation of LC3B-II (Fig.6B). This data is in agreement with our results from A549 infection experiments with the H3N2 IAV, where we observed inhibition of LC3B-II accumulation in cells treated with siRNA targeting the viral M2 transcript (Fig.6C). In the same samples, we tested the effect of M2 depletion on JNK phosphorylation and found no evidence that M2 protein was solely responsible for the activation of JNK signaling pathway (Fig.6C). On the other hand, chemical inhibition of JNK phosphorylation resulted in decrease of M2 protein levels while there was no effect on the LC3B maturation process (Fig.6C).

Altogether, data presented here demonstrate direct interaction between the viral M2 protein and LC3B that occurs on the cell membranes. The split-GFP assay shows that the IAV matrix protein recruited LC3B to the extracellular membrane and *vice versa*, the M2 protein localized at the autophagosome membranes where LC3B-II naturally resides. The viral M2 protein stimulated the LC3B lipidation required for the autophagosome maturation.

3. Discussion

411 Autophagy has been shown to significantly impact the virus life cycle, particularly the
412 fledgling phase of viral RNA synthesis [61] and presents an appealing target for host-directed
413 antiviral therapeutics. However, the role of autophagy during viral infection varies by cell type
414 and viral strain – making the critical investigation of autophagy during IAV infection, of which
415 there are an estimated 198 subtypes, uniquely challenging. Here, we evaluated the effect of IAV
416 replication on the expression profiles of genes involved in autophagy regulation and mTOR
417 signaling. The majority of *in vitro* IAV infection studies are based on cell models in which
418 autophagy activation predated virus infection. By omitting cell serum starvation during the virus
419 absorption step, we were able to capture autophagy activation during IAV infection that is more
420 representative of the events occurring *in vivo*.
421 We observed global host transcriptome changes (LFC ≥ 2) that varied between the early stages
422 of IAV replication and later timepoints depending on the ratio between infectious virus and host
423 cells, indicating that virus load played a significant role in gene expression dynamics (Fig. 1-2).
424 Despite host cells' efforts to shut down protein synthesis, IAV replication activated mTORC1
425 signaling, positively regulating protein synthesis in nutrient rich conditions. Both mTORC1 and
426 mTORC2 carry out distinct functions: activation of mTOR1 facilitates protein synthesis and
427 inhibits autophagy via repression of ULK1 signaling, while mTORC2 regulates cytoskeleton
428 dynamics and cell survival [72, 73]. Despite the activation of mTORC1, IAV replication also
429 simultaneously activated autophagy independent of ULK1 signaling. The ULK1 gene executes a
430 feedback loop between mTORC1 signaling and the autophagy pathway, inhibiting mTORC1 via
431 interaction with RPTOR during stress [74-76]. RPTOR gene activation was limited to the early
432 stages of IAV infection and may not have had the capacity to inhibit ULK1 function, particularly
433 given the continuous ULK1 transcript accumulation throughout the virus replication cycle (Fig.2

and S2). At the same time, RICTOR gene activation occurred throughout the viral replication cycle playing a major role for mTORC2 signaling in IAV infected cells [76, 77]. Our global transcriptome analysis of IAV (H3N2) infected cells revealed remarkable dependence of ULK1 and ULK2 gene activation on the viral load. At lower MOI1, the ULK1 gene was continuously activated throughout the IAV replication cycle. At MOI5, ULK1 gene expression was mostly suppressed and ULK2 was activated briefly at the early stage of IAV replication. We further examined the role of ULK1 signaling on post-transcriptional level and found that pharmacological inhibition of ULK1 had no significant effect on IAV replication and activation of autophagy in the lung cancer A549 cell line (Fig.3).

In response to increased viral burden, we observed secondary oscillatory burst of autophagy gene regulator activation as infection progressed (3-4 hpi), particularly related to protein synthesis (EIF2AK3 and MAPK3). However, at a higher viral load (MOI5) MAPK3 gene expression spiked at 3 hpi and subsequently returned to base levels. This suggests that cell stress burdened by viral protein synthesis could initiate a feedback mechanism activating MAP3K transcription. These findings implicate host cell protein synthesis downregulation as a mechanism for impeding viral replication. In turn, activation of genes regulating mTORC1 activity at early stage of IAV replication signified viral hijacking of host protein synthesis machinery (Fig.1B and 41-43). However, the steady accumulation of MAPK3/ERK (Fig.1B, MOI1) and LRP6 (Fig.2, MOI1) gene transcripts throughout IAV infection indicates that mTORC1 activation could be sustained on a post-transcriptional level (Fig. 4B: 9 hpi vs 6 hpi).

The oscillatory pattern of key autophagy (ATG7, Fig.1B, MOI1) and mTORC2 (RICTOR, Fig2, MOI1) gene expression profiles demonstrates that viral replication activates two major cell survival pathways: mTORC1 and autophagy that is independent of ULK1 signaling, also found in

Poliovirus infection [78]. This observation and the known relationship between LC3B-II and viral protein (M2) accumulation leading to autophagosome formation [44, 45], could explain an autophagy activation alternative to the classical ULK1 signaling pathways. Furthermore, our data show that pharmacological inhibition of ULK1 function prior to and upon IAV infection did not change the course of autophagy activation. Together, these results demonstrate that ULK1-independent simultaneous activation of mTORC1 and autophagy is possible when orchestrated by IAV proteins boosting their own amplification [31, 41, 43].

Previous studies have shown that direct interaction between IAV Matrix 2 (M2) ion-channel protein with LC3 blocks autophagosome fusion with lysosomes [45] and redirects LC3 to the plasma membrane to facilitate virus budding [44]. High levels of M2 responsible for accumulation of LC3II and formation of autophagosomes were linked to retardation of viral growth and decreased shedding of infectious virus particles [80]. Applying split-GFP technology, we provided direct evidence for IAV/M2-LC3 protein interaction causing localization of the LC3 to the cell wall membranes (Fig.6A). This method is superior to the derivation of protein-protein interactions from colocalization studies of LC3 and M2 fused to full-length fluorescent proteins since the fluorescent proteins tend to dimerize and produce false-positive puncta formations. We observed increased formation of autophagosomes in stable cell lines expressing LC3-GFP or LC3-Cherry fusion proteins and ruled out their application for autophagy activation studies. Thus, our study concurs with the hypothesis that the viral protein M2 is responsible for the activation of autophagy independently of the classical or alternative signaling pathway.

Additionally, we found that cell survival responses regulated by AKT-Ser473 and JNK-Thr187 became activated midway throughout the virus replication cycle. Pharmacological inhibition of JNK signaling dramatically reduced viral protein synthesis in IAV-infected NHBE

cells, while there was a modest effect in the cancer cell line A549. Our findings are in agreement with previous study reporting a key role of JNK signaling in the host cell permissiveness to Influenza virus replication. Avian IAV subtypes, H5N1 and H9N2, activated JNK signaling in chicken fibroblasts. In the same host cells, infection with the H1N1 subtype, known as swine flu causing seasonal epidemics in humans, did not activate JNK phosphorylation [81]. In our studies, we observed that both H1N1 and H3N2 subtypes activated JNK signaling in human lung cell line and this correlated with the replication efficiency of the virus (Fig.4-5 and S1D and S3C). Additionally, we observed unexpected decrease in JNK-Thr187 levels in normal human lung epithelium cultures infected with IAV (H2N3) when ULK1 signaling was targeted with a selective inhibitor SBI0206965. This could be the cause of off-target inhibition of kinases regulating JNK function in this cell type, including FAK [82-84]. Regardless, the IAV replication and production of infectious virus particles remained unchallenged compared to the experimental group treated with JNK-specific inhibitor SP600125 (Fig.5) indicating that even at reduced activity JNK signaling could support IAV infection. Only upon complete inhibition of the JNK function, was the IAV titer reduced. Collectively, our data indicate that lung carcinoma A549 show reduced sensitivity to inhibition of JNK signaling during IAV replication compared to NHBEC, supporting the idea that cell models utilized to study host-pathogen interaction would produce subjective results. Our study solidified the link between IAV infection and JNK-Thr187 signaling as a stress regulatory mechanism accompanying the rampant synthesis of viral proteins and activating alternative autophagy pathways [46-49, 81]. Therefore, therapies that decrease the host cell capacity as a viral particle “factory” through inhibition of JNK-Thr187 signaling can result in a significant reduction of infectious IAV titer.

In conclusion, our findings indicate that the IAV load is responsible for differential gene expression dynamics within the cell host. We demonstrate that IAV replication simultaneously activated transcription of key genes regulating mTORC1 and autophagy in human lung epithelial cells. Host stress response mechanisms regulated by the c-jun N-terminal kinase are co-opted by the IAV replication machinery to boost viral titer and their inhibition has the propensity to serve as host-directed antiviral therapy. We also observed differences between normal human bronchial epithelial cells and cancer cell lines in their response to virus invasion. In the search of universal, effective and safe antiviral therapies, we call for comprehensive comparison of data originating from diverse and relevant cell models of virus infection.

4. EXPERIMENTAL PROCEDURES

4.1. Cell culture, media, and chemical reagents

A549 carcinoma human alveolar epithelial cells (ATCC, CCL-185) and Madin-Darby canine kidney (MDCK) cells (ATCC, CCL-34) were maintained in high-glucose DMEM (Gibco-Thermo Fisher, Grand Island, NY) and EMEM (Gibco-Thermo Fisher, Grand Island, NY), respectively, supplemented with 10% (v/v) fetal bovine serum (Gibco-Thermo Fisher, Grand Island, NY). BEAS-2B (ATCC, CRL-9609), a polyoma virus transformed normal human lung bronchial epithelial cells, and Normal Human Bronchial Epithelial (NHBE, Lonza-CC2541) were maintained in Bronchial Epithelial Cell Growth medium obtained from Lonza/Clonetics Co as a BEGM kit (CC-3170). All cells were cultured at 37 °C and 5% CO_2.

To inhibit ULK1 signaling, A549 cells were cultured in 10%-DMEM media supplemented with 10 μM SBI0206965 (Selleckchem, Pittsburgh, PA) for 6 hours prior to IAV infection, and drug concentration was maintained in the media post-virus infection. Since BEAS-2B and NHBE

have lower expression levels of ULK1, SBI0206965 was added at 1 μM to the BEGM growth media. We observed high toxicity at 10 μM SBI0206965 for both non-carcinoma cell types, which could be caused by an off-target drug effect at this concentration. To inhibit JNK-Thr187 phosphorylation, we added 10 μM SP600125 (Selleckchem, Pittsburgh, PA) to A549 growth media 6 hours prior to IAV infection, while 5 μM and 1 μM were added to the culture media of NHBE and BEAS-2B, respectively, due to sensitivity issues resulting from JNK inhibition.

4.2. Viruses and Virus infection procedures

The following IAV strains were used in this study: *A/PR/8/1934* (H1N1) and *A/Port Chalmers/1/73* (H3N2). The virus work was performed in compliance with CDC guidelines for biosafety level 2 agents. Virus stocks were prepared from MDCK cells infected at MOI of 0.01 in the following media: EMEM, 10 mM HEPES (Gibco), 0.125% BSA (Gibco), 1 μg/mL TPCK trypsin (Worthington Biomedical Corporation). MDCK cells were incubated for 1 hour at 37 °C in virus media, washed with PBS, and overlaid with serum free EMEM containing 1 μg/mL TPCK trypsin. Conditioned media was harvested when a cytopathic effect was observed (usually 24 and 48 hpi for *A/PCh/1/73* and, *A/PR/8/34* respectively), centrifuged at 1,000 g for 10 minutes, passed through 0.45 μm Nalgene filter units, and aliquoted in 50% BSA media for storage at -80 °C. The virus titer was determined in MDCK cells by plaque assays, as described previously [50], and immunoplaque analysis was performed with anti-NP antibody (ThermoFisher, PA5-32242) and alkaline phosphatase conjugated anti-rabbit antibody.

To study the dynamics of viral RNA replication, A549 cells were plated 18 hours prior to infection in high glucose DMEM supplemented with 5% or 10% Fetal clone III serum at $1x10^6$ per well in 6-well format dishes. In order to standardize the multiplicity of virus infection (MOI) between independent virus infection experiments, the cell number was calculated from a control

547 sample immediately before IAV infection. A549 cells were mock treated in 6-well plates with
548 virus free media or were infected with 250 µL virus containing media. To compare the effect of
549 serum starvation on autophagy activation we utilized two protocols of virus activation for
550 absorption.

551 The serum-starved protocol has been broadly used in *in vitro* IAV infections and is based on
552 dilution of viral stocks in serum free media supplemented with 1 µg/mL TPCK trypsin followed
553 by incubation of virus media and host cells for 1 hour at 37◦C. After 1 hour, 1 ml of EMEM
554 supplemented with 5% Fetal clone III serum (5% DMEM) was added and cells were incubated at
555 37 °C prior to harvest.

556 In the serum replete protocol, 20 µg TPCK-treated trypsin (Warthington, Lakewood, NJ) was
557 added to 1 ml virus stock (harvested from MDCK producer cells in serum free media) and was
558 incubated for 10 minutes at 37 °C to activate cleavage of viral HA glycoprotein to HA1 and HA2.
559 Equal volume (1 v/v) of EMEM supplemented with 10% Fetal clone III serum (10% EMEM) was
560 added to the TPCK trypsin-treated virus to neutralize the enzyme. To determine the titer of
561 infectious IAV particles, 250 µL of the trypsin pre-activated virus diluted to $2x10^5$ (approximated
562 from the pfu/ml of the original virus stock) in 10%-EMEM were layered over $2x10^6$ MDCK cells
563 in a 6-well plate and incubated for 1h at 37 °C. In parallel, 250 µL of the original virus stock diluted
564 to MOI 0.1 in serum-free EMEM supplemented with 1 µg/mL TPCK-treated trypsin was layered
565 over $2x10^6$ MDCK cells in a 6-well plate and incubated for 1h at 37 °C. Following the 1h virus
566 absorption step, 2 mL 10%-EMEM were added to the infected cells and the incubation at 37 °C
567 continued for 48h. Conditioned media from IAV-infected MDCK cells was serially diluted (log10)
568 in serum-free EMEM media supplemented with 1 µg/mL TPCK-treated trypsin to determine the
569 virus titer in MDCK cells by plaque assays, as described previously [50]. On average, the titer

570 (pfu/mL) produced by cells infected with trypsin pre-activated IAV in serum replete media was
571 10-fold lower compared to the infections in serum-free media. To normalize the MOI between the
572 two protocols, A549 cells were infected at 10-fold higher virus titer for the serum replete protocol
573 compared to the serum-free protocol. Cells were collected at 1, 3, 6 and 8h post-infection and the
574 levels of viral RNA were determined via quantitative RT-PCR with Taqman probe (5'-/56-
575 FAM/AGCTCTCGG/ZEN/ACGAARGGCARCGA/3IABkFQ/-3') and primers (5'-
576 TCCTCTGCATTGTCTCCGAA-3' and 5'-TGTCYTTYCAGGGGCGGG-3') targeting the IAV
577 NP6 transcript. With this quantitative method, we observed comparable levels of viral transcripts
578 (ΔCt normalized to GAPDH transcripts) between the two infection protocols when 10-fold higher
579 virus titer was applied in the serum-replete protocol. For the transcriptome and WB studies, A549
580 cells were plated 18 hours prior to infection in 10% DMEM at $1x10^6$ per well in 6-well format
581 dishes. Pre-activated virus stock was adjusted to the required MOI in 10% DMEM and was layered
582 on target cells at 250 µL. After 1 hour of incubation at 37 °C, A549 mock and virus infected cells
583 were topped with fresh 10%-DMEM to a total volume of 2 mL and were incubated at 37 °C prior
584 to harvest.

585 *4.3. RNA isolation and sample preparation for Illumina RNA Mi-seq analysis.*

586 At indicated time points, post initiation of infection, cells were washed with cold phosphate
587 buffered saline (PBS) and lysed in the well with 350 µL 1% beta-mercaptoethanol supplemented
588 RLT buffer from the RNeasy Plus Mini kit (QIAGEN, Maryland). Total RNA was isolated
589 according to the manufacturer's protocol, including on-column removal of gDNA. After elution,
590 total RNA was treated with Turbo DNA-free Kit (AM1907, Thermo Fisher Scientific) for
591 complete elimination of gDNA. RNA quality was determined by both direct observation of rRNA
592 on 1% denaturing agarose gel and by Agilent bioanalyzer scan. For the preparation of Illumina

libraries, 5 µg total RNA per sample was processed with the TruSeq Stranded Total RNA Ribo-Zero H/M/R kit (RS-122-2201, Illumina). Following rRNA removal, polyA-mRNA species were separated from the non-polyA RNA pool with the polyA Spin mRNA Isolation Kit (S1560S, NEB). The two RNA sample pools were further quantified by Qubit (Invitrogen) and 15 ng were subjected to size fragmentation followed by cDNA synthesis and the addition of a terminal tagged oligonucleotide. Tagged cDNA was purified with Agencourt AMpure XP beads and amplified with 15 cycles of PCR. Fragment length distribution of all libraries was analyzed on a BioAnalyzer high-sensitivity LabChip. Diluted libraries (5 pmol) were multiplexed and sequenced on the Illumina MiSeq (2- by 250-bp paired-end run with 3 to 4 million reads/sample).

4.4. Analysis of RNAseq data and differential gene expression assay

RNAseq data was analyzed on the EDGE Bioinformatics platform [51]. Using the PiReT application (https://github.com/mshakya/piret), we performed quality control on the RNA-seq data using FaQC v2.09 [52]. The reads that passed the QC were mapped using HISAT2 v2.1.0 against its graph FM index (GFM) human reference genome [53]. Htseq-count v0.11.1 was used to calculate the number of reads mapped to coding sequences [54]. Applying count data, we calculated transcripts per kilobase per million (TPM) and found differentially expressed genes using the R package DESeq2 v1.18.1. Heatmaps showing fold change (FC) were made using the R package heatmap v1.0.10 which clustered both rows and columns based on FC values.

4.5. Data availability.

All transcriptomics data have been submitted to GEO under accession number GSE162295 (https://www.ncbi.nlm.nih.gov/geo/query/acc.cgi?acc=GSE162295) and NCBI tracking system #21497852.

615 *4.6. Western blot analysis and Fluorescent Microscopy*

616 Uninfected cells and cells infected with *A/Port Chalmers/1/73* (H3N2) at MOI5 were
617 collected after the treatment of interest and were solubilized in RIPA Lysis and Extraction Buffer
618 (Thermo Scientific, Grand Island, NY) supplemented with a cocktail of protease and phosphatase
619 inhibitor mixture (Thermo Scientific). Lysates were cleared at 14,000 rpm for 15 minutes, and the
620 total protein amount in the supernatants was quantified with the BCA kit (Pierce). Equal amounts
621 of protein (5 μg) were resolved by Tris-Glycine-SDS PAGE electrophoresis (4-15% Mini-
622 PROTEAN, BioRad, Hercules, CA). After the SDS-PAGE the proteins were transferred onto
623 PVDF membranes (Millipore, Billerica, MA), blocked with 5% nonfat dried milk in TBST (25
624 mM Tris [pH 7.6], 137 mM NaCl, and 0.2% Tween 20) and incubated overnight at 4 °C with
625 primary antibodies in 1% bovine serum albumin in phosphate buffered saline. Membranes washed
626 from the primary antibodies were incubated for 2 hours in HRP-conjugated secondary antibody
627 and were analyzed for immunoreactive proteins with luminol reagent (Santa Cruz Biotechnology)
628 by BioRad Molecular Imager ChemiDoc XRS+. Image Lab 6.0 software was applied for
629 quantitative analysis of the protein band intensity. The following primary antibodies were used in
630 this study: anti-actin (sc-58673, 2Q1055); anti-Influenza A Virus M2 Protein [14C2] (ab5416);
631 anti-Influenza A Virus Nucleoprotein [9C11] (SAB5300169); anti-LC3B (CST-2775); anti-mTOR
632 [7C10] (CST-2983); anti-phospho-mTOR(S2448) [D9C2] (CST-5536); anti-ULK1 [D8H5] (CST-
633 8054); anti-phospho-ULK1(S757) [D706U] (CST-14202); anti-SAPK/JNK (CST-9252); anti-
634 phospho-SAPK/JNK(Thr183/Tyr185) (CST-9251).

635 For the fluorescent microscopy studies, cells were plated on borosilicate chamber slides pre-
636 coated with fibronectin. IAV-infected and mock-treated samples were fixed with 4%
637 paraformaldehyde at various time points, incubated in blocking solution (PBS+3% bovine serum

albumin) and labeled with mouse anti-Influenza A Virus M2 Protein [14C2] (ab5416). Following overnight incubation with the anti-IVA/M2 primary antibody, cells were washed in PBS and permeabilized (PBS+0.25% TritonX) prior to incubation with rabbit anti-LC3B antibody (Sigma, L7543). Alexa Fluor488 goat anti-mouse (ab150113) and Alexa Fluor555 goat anti-rabbit IgGs were used to fluorescently label IVA/M2 and LC3B proteins, respectively. Images were obtained from Zeiss Axio Observer.Z1 using ZenPro software. To determine the percentage of infected cells, images with fluorescently labeled anti-IVA/M2 antibody were obtained with 20x objective choosing fields with > 300 cells. For each culture condition, 5 images were taken from non-overlapping fields and were analyzed with ImageJ. A cell counter plugin was created with the following parameters: (i) manual threshold, (ii) fill holes, (iii) enhance contrast and saturated pixels at 0.3%, (iv) watershed separation, and (v) particle analysis at size 100-infinity and circularity at 0.2–0.1. The fraction of cells labeled with anti-viral antibody was calculated as percent of total cell population labeled with DAPI.

4.7. ELISA

Endogenous levels of phosphorylated AKT at Ser473 were determined with FastScan™ Phospho-Akt (Ser473) ELISA Kit (Cell Signaling technologies, CST#80895) in cleared cell lysates of mock treated and virus infected 10^6 A549 cells. Absolute values of phosphorylated Ser473-AKT were determined with a standard curve correlating the positive control phospho-Akt(Ser473) concentration (μg/mL) to absorbance at 450 nM. We utilized PathScan Phospho-p70 S6 Kinase (Thr389) Sandwich ELISA kit (Cell Signaling technologies, CST#7063) to determine mTORC1 activity by measuring the phosphorylated levels of its primary substrate p70S6K. In this assay the levels of phosphorylated Thr389 (detection antibody) were normalized to the total levels

660 of p70S6K protein (capture antibody). A Bioteck Synergy 2 plate reader was used to collect
661 absorbance at 450 nm.

662 *4.8. Plasmids and reagents for split-GFP in situ protein-protein interactions*

663 To study direct interaction of IAV M2 and host LC3B proteins, we used a split green
664 fluorescent protein (GFP) assay, as previously described [55]. gBLOCK Gene Fragments,
665 encoding for GFP11- and GFP10-tagged M2 and LC3B, were chemically synthesized by Twist
666 Biosciences Inc. The synthetic DNA contained a set of primer sequences for amplification and
667 Hind III and EcoR V restriction enzyme sites. The genes also contained methionine required for
668 the start and a stop codon. The 5' end of all gene constructs contained
669 CGATTAACGGTCTCTGGGGAAGCTTACCATG the 3'end of the sequences contained
670 TAAGATATCAAAAGGAGACCGTTAATCTAAAATCATTATTTG. The primers used for
671 amplification of the constructs were forward primer CGATTAACGGTCTCTGGGG and reverse
672 primer CAAATAATGATTTTAGATTAACGG. All genes were PCR amplified using Q5 proof
673 reading polymerase (New England Biolabs, M0491). Purified PCR products encoding the GFP
674 Tag were cloned into a pcDNA 5.1 vector plasmid encoding influenza A M2 protein [56].
675 Restriction enzymes Hind III (NEB, #R0104) and EcoRV (NEB # R0195) were used to create
676 sticky ends on the PCR and plasmid vector, followed by gel extraction and purification (Qiagen
677 #28706) prior to T4 DNA (NEB, #B0202) ligation. The plasmid vectors encoding tagged-M2 and
678 LC3B proteins were verified via Sanger sequencing, and the amino acid sequence of the various
679 constructs are presented in Supplementary material (S3). For the Split GFP assay, the plasmid
680 vectors encoding for tagged M2 and LC3B proteins were transfected in HEK293T cells with
681 Lipofectamine 3000 (Thermo Fisher/Invitrogen). At day 3 post-transfection, the cells were fixed
682 with 4% paraformaldehyde (15 minutes at room temperature) and permeabilized with 0.3% Triton

X100 (10 minutes at room temperature). After blocking with 2% BSA in phosphate buffer saline (PBS), the cells were incubated overnight at 4 ℃ with purified protein fraction of GFP1-9 (10 μg/mL). Only when in very close proximity the GFP11 and GFP10 peptides can be complimented with the larger fraction GFP1-9 to produce folded and fluorescent GFP [57]. Imaging was performed on Zeiss Axio Observer.Z1 and processed with ZenPro software.

Author Contributions: conceptualization, S. M-V. and T.A.S.B; methodology, S. M-V., T.A.S.B, N.V., C. D.G., and S.B.; formal analysis, S. M-V., T.A.S.B, S.R.S., and G.X.; investigation, S. M-V., T.A.S.B., S.R.S., and N.V.; writing – original draft preparation, S. M-V. and T.A.S.B.; writing – review and editing, S. M-V., T.A.S.B., and N.V.; supervision, S.M-V., S.R.S., and G.W.; funding acquisition, S.M-V., G.W., and S.R.S.

Funding: Funding for this work was provided by Los Alamos National Laboratory R&D grants 202000696ER to S.M-V., 20160054DR to G.W., and 20210082DR to S.R.S.

Conflicts of Interest: The authors declare no conflict of interest

REFERENCES

1. Shang, L.; Chen, S.; Du, F.; Li, S.; Zhao, L.; Wang, X., Nutrient starvation elicits an acute autophagic response mediated by Ulk1 dephosphorylation and its subsequent dissociation from AMPK. *Proc Natl Acad Sci U S A* **2011,** *108* (12), 4788-4793.
2. Kim, J.; Kundu, M.; Viollet, B.; Guan, K. L., AMPK and mTOR regulate autophagy through direct phosphorylation of Ulk1. *Nat Cell Biol* **2011,** *13* (2), 132-41.
3. Qiang, L.; Sample, A.; Shea, C. R.; Soltani, K.; Macleod, K. F.; He, Y.-Y., Autophagy gene ATG7 regulates ultraviolet radiation-induced inflammation and skin tumorigenesis. *Autophagy* **2017,** *13* (12), 2086-2103.
4. Hussey, S.; Travassos, L. H.; Jones, N. L., Autophagy as an emerging dimension to adaptive and innate immunity. *Seminars in Immunology* **2009,** *21* (4), 233-241.
5. Kuballa, P.; Nolte, W. M.; Castoreno, A. B.; Xavier, R. J., Autophagy and the Immune System. *Annual Review of Immunology* **2012,** *30* (1), 611-646.
6. Siqueira, M. d. S.; Ribeiro, R. d. M.; Travassos, L. H., Autophagy and Its Interaction With Intracellular Bacterial Pathogens. *Frontiers in immunology* **2018,** *9*, 935-935.
7. Kim, Y. S.; Silwal, P.; Kim, S. Y.; Yoshimori, T.; Jo, E.-K., Autophagy-activating strategies to promote innate defense against mycobacteria. *Experimental & Molecular Medicine* **2019,** *51* (12), 1-10.
8. Abdulrahman, B. A.; Khweek, A. A.; Akhter, A.; Caution, K.; Kotrange, S.; Abdelaziz, D. H. A.; Newland, C.; Rosales-Reyes, R.; Kopp, B.; McCoy, K.; Montione, R.; Schlesinger, L. S.; Gavrilin, M. A.; Wewers, M. D.; Valvano, M. A.; Amer, A. O., Autophagy stimulation by rapamycin suppresses lung inflammation and infection by Burkholderia cenocepacia in a model of cystic fibrosis. *Autophagy* **2011,** *7* (11), 1359-1370.
9. Paul, P.; Münz, C., Autophagy and Mammalian Viruses: Roles in Immune Response, Viral Replication, and Beyond. *Adv Virus Res* **2016,** *95*, 149-95.
10. Deretic, V.; Saitoh, T.; Akira, S., Autophagy in infection, inflammation and immunity. *Nature Reviews Immunology* **2013,** *13* (10), 722-737.

11. Saitoh, T.; Fujita, N.; Jang, M. H.; Uematsu, S.; Yang, B. G.; Satoh, T.; Omori, H.; Noda, T.; Yamamoto, N.; Komatsu, M.; Tanaka, K.; Kawai, T.; Tsujimura, T.; Takeuchi, O.; Yoshimori, T.; Akira, S., Loss of the autophagy protein Atg16L1 enhances endotoxin-induced IL-1beta production. *Nature* **2008,** *456* (7219), 264-8.
12. Harris, J.; Hartman, M.; Roche, C.; Zeng, S. G.; O'Shea, A.; Sharp, F. A.; Lambe, E. M.; Creagh, E. M.; Golenbock, D. T.; Tschopp, J.; Kornfeld, H.; Fitzgerald, K. A.; Lavelle, E. C., Autophagy controls IL-1beta secretion by targeting pro-IL-1beta for degradation. *J Biol Chem* **2011,** *286* (11), 9587-97.
13. Valečka, J.; Almeida, C. R.; Su, B.; Pierre, P.; Gatti, E., Autophagy and MHC-restricted antigen presentation. *Mol Immunol* **2018,** *99*, 163-170.
14. Mintern, J. D.; Macri, C.; Chin, W. J.; Panozza, S. E.; Segura, E.; Patterson, N. L.; Zeller, P.; Bourges, D.; Bedoui, S.; McMillan, P. J.; Idris, A.; Nowell, C. J.; Brown, A.; Radford, K. J.; Johnston, A. P.; Villadangos, J. A., Differential use of autophagy by primary dendritic cells specialized in cross-presentation. *Autophagy* **2015,** *11* (6), 906-17.
15. Levine, B.; Kroemer, G., Biological Functions of Autophagy Genes: A Disease Perspective. *Cell* **2019,** *176* (1-2), 11-42.
16. Mizushima, N.; Yoshimori, T.; Levine, B., Methods in mammalian autophagy research. *Cell* **2010,** *140* (3), 313-326.
17. Liang, X. H.; Kleeman, L. K.; Jiang, H. H.; Gordon, G.; Goldman, J. E.; Berry, G.; Herman, B.; Levine, B., Protection against fatal Sindbis virus encephalitis by beclin, a novel Bcl-2-interacting protein. *J Virol* **1998,** *72* (11), 8586-96.
18. Campbell, G. R.; Spector, S. A., Hormonally active vitamin D3 (1alpha,25-dihydroxycholecalciferol) triggers autophagy in human macrophages that inhibits HIV-1 infection. *J Biol Chem* **2011,** *286* (21), 18890-902.
19. Shoji-Kawata, S.; Sumpter, R.; Leveno, M.; Campbell, G. R.; Zou, Z.; Kinch, L.; Wilkins, A. D.; Sun, Q.; Pallauf, K.; MacDuff, D.; Huerta, C.; Virgin, H. W.; Helms, J. B.; Eerland, R.; Tooze, S. A.; Xavier, R.; Lenschow, D. J.; Yamamoto, A.; King, D.; Lichtarge, O.; Grishin, N. V.; Spector, S. A.; Kaloyanova, D. V.; Levine, B., Identification of a candidate therapeutic autophagy-inducing peptide. *Nature* **2013,** *494* (7436), 201-206.
20. Kobayashi, S.; Yoshii, K.; Phongphaew, W.; Muto, M.; Hirano, M.; Orba, Y.; Sawa, H.; Kariwa, H., West Nile virus capsid protein inhibits autophagy by AMP-activated protein kinase degradation in neurological disease development. *PLoS Pathog* **2020,** *16* (1), e1008238-e1008238.
21. Levine, B.; Mizushima, N.; Virgin, H. W., Autophagy in immunity and inflammation. *Nature* **2011,** *469* (7330), 323-335.
22. Li, J.; Liu, Y.; Wang, Z.; Liu, K.; Wang, Y.; Liu, J.; Ding, H.; Yuan, Z., Subversion of cellular autophagy machinery by hepatitis B virus for viral envelopment. *Journal of virology* **2011,** *85* (13), 6319-6333.
23. Starr, T.; Child, R.; Wehrly, T. D.; Hansen, B.; Hwang, S.; López-Otin, C.; Virgin, H. W.; Celli, J., Selective subversion of autophagy complexes facilitates completion of the Brucella intracellular cycle. *Cell Host Microbe* **2012,** *11* (1), 33-45.
24. Kyei, G. B.; Dinkins, C.; Davis, A. S.; Roberts, E.; Singh, S. B.; Dong, C.; Wu, L.; Kominami, E.; Ueno, T.; Yamamoto, A.; Federico, M.; Panganiban, A.; Vergne, I.; Deretic, V., Autophagy pathway intersects with HIV-1 biosynthesis and regulates viral yields in macrophages. *The Journal of cell biology* **2009,** *186* (2), 255-268.
25. Sriwilaijaroen, N.; Suzuki, Y., Host Receptors of Influenza Viruses and Coronaviruses-Molecular Mechanisms of Recognition. *Vaccines (Basel)* **2020,** *8* (4).
26. Smith, G. J.; Vijaykrishna, D.; Bahl, J.; Lycett, S. J.; Worobey, M.; Pybus, O. G.; Ma, S. K.; Cheung, C. L.; Raghwani, J.; Bhatt, S.; Peiris, J. S.; Guan, Y.; Rambaut, A., Origins and evolutionary genomics of the 2009 swine-origin H1N1 influenza A epidemic. *Nature* **2009,** *459* (7250), 1122-5.
27. Viboud, C.; Gostic, K.; Nelson, M. I.; Price, G. E.; Perofsky, A.; Sun, K.; Sequeira Trovão, N.; Cowling, B. J.; Epstein, S. L.; Spiro, D. J., Beyond clinical trials: Evolutionary and epidemiological considerations for development of a universal influenza vaccine. *PLoS Pathog* **2020,** *16* (9), e1008583-e1008583.
28. Nelson, M. I.; Simonsen, L.; Viboud, C.; Miller, M. A.; Holmes, E. C., The origin and global emergence of adamantane resistant A/H3N2 influenza viruses. *Virology* **2009,** *388* (2), 270-8.

29. Simonsen, L.; Viboud, C.; Grenfell, B. T.; Dushoff, J.; Jennings, L.; Smit, M.; Macken, C.; Hata, M.; Gog, J.; Miller, M. A.; Holmes, E. C., The genesis and spread of reassortment human influenza A/H3N2 viruses conferring adamantane resistance. *Mol Biol Evol* **2007,** *24* (8), 1811-20.
30. Sun, Y.; Li, C.; Shu, Y.; Ju, X.; Zou, Z.; Wang, H.; Rao, S.; Guo, F.; Liu, H.; Nan, W.; Zhao, Y.; Yan, Y.; Tang, J.; Zhao, C.; Yang, P.; Liu, K.; Wang, S.; Lu, H.; Li, X.; Tan, L.; Gao, R.; Song, J.; Gao, X.; Tian, X.; Qin, Y.; Xu, K.-F.; Li, D.; Jin, N.; Jiang, C., Inhibition of Autophagy Ameliorates Acute Lung Injury Caused by Avian Influenza A H5N1 Infection. *Science Signaling* **2012,** *5* (212), ra16.
31. Kuss-Duerkop, S. K.; Wang, J.; Mena, I.; White, K.; Metreveli, G.; Sakthivel, R.; Mata, M. A.; Muñoz-Moreno, R.; Chen, X.; Krammer, F.; Diamond, M. S.; Chen, Z. J.; García-Sastre, A.; Fontoura, B. M. A., Influenza virus differentially activates mTORC1 and mTORC2 signaling to maximize late stage replication. *PLoS Pathog* **2017,** *13* (9), e1006635-e1006635.
32. Zhou, Z.; Jiang, X.; Liu, D.; Fan, Z.; Hu, X.; Yan, J.; Wang, M.; Gao, G. F., Autophagy is involved in influenza A virus replication. *Autophagy* **2009,** *5* (3), 321-8.
33. Zhirnov, O. P.; Klenk, H. D., Influenza A virus proteins NS1 and hemagglutinin along with M2 are involved in stimulation of autophagy in infected cells. *J Virol* **2013,** *87* (24), 13107-14.
34. Ma, X. M.; Blenis, J., Molecular mechanisms of mTOR-mediated translational control. *Nat Rev Mol Cell Biol* **2009,** *10* (5), 307-18.
35. Laplante, M.; Sabatini, D. M., mTOR signaling in growth control and disease. *Cell* **2012,** *149* (2), 274-93.
36. Jung, C. H.; Jun, C. B.; Ro, S. H.; Kim, Y. M.; Otto, N. M.; Cao, J.; Kundu, M.; Kim, D. H., ULK-Atg13-FIP200 complexes mediate mTOR signaling to the autophagy machinery. *Mol Biol Cell* **2009,** *20* (7), 1992-2003.
37. Ganley, I. G.; Lam du, H.; Wang, J.; Ding, X.; Chen, S.; Jiang, X., ULK1.ATG13.FIP200 complex mediates mTOR signaling and is essential for autophagy. *J Biol Chem* **2009,** *284* (18), 12297-305.
38. Ma, J.; Sun, Q.; Mi, R.; Zhang, H., Avian influenza A virus H5N1 causes autophagy-mediated cell death through suppression of mTOR signaling. *J Genet Genomics* **2011,** *38* (11), 533-7.
39. Zhang, C.; Yang, Y.; Zhou, X.; Liu, X.; Song, H.; He, Y.; Huang, P., Highly pathogenic avian influenza A virus H5N1 NS1 protein induces caspase-dependent apoptosis in human alveolar basal epithelial cells. *Virol J* **2010,** *7*, 51.
40. Lam, W. Y.; Tang, J. W.; Yeung, A. C.; Chiu, L. C.; Sung, J. J.; Chan, P. K., Avian influenza virus A/HK/483/97(H5N1) NS1 protein induces apoptosis in human airway epithelial cells. *J Virol* **2008,** *82* (6), 2741-51.
41. Zhirnov, O. P.; Klenk, H. D., Control of apoptosis in influenza virus-infected cells by up-regulation of Akt and p53 signaling. *Apoptosis* **2007,** *12* (8), 1419-32.
42. Ehrhardt, C.; Wolff, T.; Pleschka, S.; Planz, O.; Beermann, W.; Bode, J. G.; Schmolke, M.; Ludwig, S., Influenza A virus NS1 protein activates the PI3K/Akt pathway to mediate antiapoptotic signaling responses. *J Virol* **2007,** *81* (7), 3058-67.
43. Shin, Y. K.; Li, Y.; Liu, Q.; Anderson, D. H.; Babiuk, L. A.; Zhou, Y., SH3 binding motif 1 in influenza A virus NS1 protein is essential for PI3K/Akt signaling pathway activation. *J Virol* **2007,** *81* (23), 12730-9.
44. Beale, R.; Wise, H.; Stuart, A.; Ravenhill, B. J.; Digard, P.; Randow, F., A LC3-interacting motif in the influenza A virus M2 protein is required to subvert autophagy and maintain virion stability. *Cell Host Microbe* **2014,** *15* (2), 239-47.
45. Gannagé, M.; Dormann, D.; Albrecht, R.; Dengjel, J.; Torossi, T.; Rämer, P. C.; Lee, M.; Strowig, T.; Arrey, F.; Conenello, G.; Pypaert, M.; Andersen, J.; García-Sastre, A.; Münz, C., Matrix protein 2 of influenza A virus blocks autophagosome fusion with lysosomes. *Cell Host Microbe* **2009,** *6* (4), 367-80.
46. Eliopoulos, A. G.; Blake, S. M.; Floettmann, J. E.; Rowe, M.; Young, L. S., Epstein-Barr virus-encoded latent membrane protein 1 activates the JNK pathway through its extreme C terminus via a mechanism involving TRADD and TRAF2. *J Virol* **1999,** *73* (2), 1023-35.
47. McLean, T. I.; Bachenheimer, S. L., Activation of cJUN N-terminal kinase by herpes simplex virus type 1 enhances viral replication. *J Virol* **1999,** *73* (10), 8415-26.
48. Clarke, P.; Meintzer, S. M.; Widmann, C.; Johnson, G. L.; Tyler, K. L., Reovirus infection activates JNK and the JNK-dependent transcription factor c-Jun. *J Virol* **2001,** *75* (23), 11275-83.

49. Nacken, W.; Anhlan, D.; Hrincius, E. R.; Mostafa, A.; Wolff, T.; Sadewasser, A.; Pleschka, S.; Ehrhardt, C.; Ludwig, S., Activation of c-jun N-terminal kinase upon influenza A virus (IAV) infection is independent of pathogen-related receptors but dependent on amino acid sequence variations of IAV NS1. *J Virol* **2014,** *88* (16), 8843-52.
50. Szretter, K. J.; Balish, A. L.; Katz, J. M., Influenza: Propagation, Quantification, and Storage. *Current Protocols in Microbiology* **2006,** *3* (1), 15G.1.1-15G.1.22.
51. Li, P. E.; Lo, C. C.; Anderson, J. J.; Davenport, K. W.; Bishop-Lilly, K. A.; Xu, Y.; Ahmed, S.; Feng, S.; Mokashi, V. P.; Chain, P. S., Enabling the democratization of the genomics revolution with a fully integrated web-based bioinformatics platform. *Nucleic Acids Res* **2017,** *45* (1), 67-80.
52. Lo, C.-C.; Chain, P. S. G., Rapid evaluation and quality control of next generation sequencing data with FaQCs. *BMC Bioinformatics* **2014,** *15* (1), 366.
53. Kim, D.; Paggi, J. M.; Park, C.; Bennett, C.; Salzberg, S. L., Graph-based genome alignment and genotyping with HISAT2 and HISAT-genotype. *Nature Biotechnology* **2019,** *37* (8), 907-915.
54. Anders, S.; Pyl, P. T.; Huber, W., HTSeq—a Python framework to work with high-throughput sequencing data. *Bioinformatics* **2015,** *31* (2), 166-169.
55. Cabantous, S.; Terwilliger, T. C.; Waldo, G. S., Protein tagging and detection with engineered self-assembling fragments of green fluorescent protein. *Nature Biotechnology* **2005,** *23* (1), 102-107.
56. Gabbard, J.; Velappan, N.; Di Niro, R.; Schmidt, J.; Jones, C. A.; Tompkins, S. M.; Bradbury, A. R. M., A humanized anti-M2 scFv shows protective in vitro activity against influenza. *Protein Engineering, Design and Selection* **2009,** *22* (3), 189-198.
57. Cabantous, S.; Nguyen, H. B.; Pedelacq, J.-D.; Koraïchi, F.; Chaudhary, A.; Ganguly, K.; Lockard, M. A.; Favre, G.; Terwilliger, T. C.; Waldo, G. S., A New Protein-Protein Interaction Sensor Based on Tripartite Split-GFP Association. *Scientific Reports* **2013,** *3* (1), 2854.
58. Zhirnov, O. P.; Ikizler, M. R.; Wright, P. F., Cleavage of Influenza A Virus Hemagglutinin in Human Respiratory Epithelium Is Cell Associated and Sensitive to Exogenous Antiproteases. *Journal of Virology* **2002,** *76* (17), 8682.
59. Klenk, H.-D.; Garten, W., Host cell proteases controlling virus pathogenicity. *Trends in Microbiology* **1994,** *2* (2), 39-43.
60. Steinhauer, D. A., Role of Hemagglutinin Cleavage for the Pathogenicity of Influenza Virus. *Virology* **1999,** *258* (1), 1-20.
61. Wang, R.; Zhu, Y.; Zhao, J.; Ren, C.; Li, P.; Chen, H.; Jin, M.; Zhou, H., Autophagy Promotes Replication of Influenza A Virus In Vitro. *Journal of virology* **2019,** *93* (4), e01984-18.
62. Napolitano, G.; Ballabio, A., TFEB at a glance. *Journal of Cell Science* **2016,** *129* (13), 2475.
63. Carriere, A.; Romeo, Y.; Acosta-Jaquez, H. A.; Moreau, J.; Bonneil, E.; Thibault, P.; Fingar, D. C.; Roux, P. P., ERK1/2 phosphorylate Raptor to promote Ras-dependent activation of mTOR complex 1 (mTORC1). *The Journal of biological chemistry* **2011,** *286* (1), 567-577.
64. Zoncu, R.; Efeyan, A.; Sabatini, D. M., mTOR: from growth signal integration to cancer, diabetes and ageing. *Nat Rev Mol Cell Biol* **2011,** *12* (1), 21-35.
65. Xu, F.; Na, L.; Li, Y.; Chen, L., Roles of the PI3K/AKT/mTOR signalling pathways in neurodegenerative diseases and tumours. *Cell & Bioscience* **2020,** *10* (1), 54.
66. Mendoza, M. C.; Er, E. E.; Blenis, J., The Ras-ERK and PI3K-mTOR pathways: cross-talk and compensation. *Trends Biochem Sci* **2011,** *36* (6), 320-328.
67. Inoki, K.; Ouyang, H.; Zhu, T.; Lindvall, C.; Wang, Y.; Zhang, X.; Yang, Q.; Bennett, C.; Harada, Y.; Stankunas, K.; Wang, C.-y.; He, X.; MacDougald, O. A.; You, M.; Williams, B. O.; Guan, K.-L., TSC2 Integrates Wnt and Energy Signals via a Coordinated Phosphorylation by AMPK and GSK3 to Regulate Cell Growth. *Cell* **2006,** *126* (5), 955-968.
68. Raciti, M.; Lotti, L. V.; Valia, S.; Pulcinelli, F. M.; Di Renzo, L., JNK2 is activated during ER stress and promotes cell survival. *Cell Death & Disease* **2012,** *3* (11), e429-e429.
69. Wei, Y.; Pattingre, S.; Sinha, S.; Bassik, M.; Levine, B., JNK1-mediated phosphorylation of Bcl-2 regulates starvation-induced autophagy. *Mol Cell* **2008,** *30* (6), 678-688.

70. Yamamoto, K.; Ichijo, H.; Korsmeyer, S. J., BCL-2 Is Phosphorylated and Inactivated by an ASK1/Jun N-Terminal Protein Kinase Pathway Normally Activated at G₂/M. *Molecular and Cellular Biology* **1999,** *19* (12), 8469.
71. Holsinger, L. J.; Lamb, R. A., Influenza virus M2 integral membrane protein is a homotetramer stabilized by formation of disulfide bonds. *Virology* **1991,** *183* (1), 32-43.
72. Sabatini, D. M., Twenty-five years of mTOR: Uncovering the link from nutrients to growth. *Proceedings of the National Academy of Sciences* **2017,** *114* (45), 11818.
73. Oh, W. J.; Jacinto, E., mTOR complex 2 signaling and functions. *Cell Cycle* **2011,** *10* (14), 2305-2316.
74. Jung, C. H.; Seo, M.; Otto, N. M.; Kim, D. H., ULK1 inhibits the kinase activity of mTORC1 and cell proliferation. *Autophagy* **2011,** *7* (10), 1212-21.
75. Dunlop, E. A.; Hunt, D. K.; Acosta-Jaquez, H. A.; Fingar, D. C.; Tee, A. R., ULK1 inhibits mTORC1 signaling, promotes multisite Raptor phosphorylation and hinders substrate binding. *Autophagy* **2011,** *7* (7), 737-747.
76. Luo, Y.; Xu, W.; Li, G.; Cui, W., Weighing In on mTOR Complex 2 Signaling: The Expanding Role in Cell Metabolism. *Oxidative Medicine and Cellular Longevity* **2018,** *2018*, 7838647.
77. Sarbassov, D. D.; Ali, S. M.; Kim, D. H.; Guertin, D. A.; Latek, R. R.; Erdjument-Bromage, H.; Tempst, P.; Sabatini, D. M., Rictor, a novel binding partner of mTOR, defines a rapamycin-insensitive and raptor-independent pathway that regulates the cytoskeleton. *Curr Biol* **2004,** *14* (14), 1296-302.
78. Corona Velazquez, A.; Corona, A. K.; Klein, K. A.; Jackson, W. T., Poliovirus induces autophagic signaling independent of the ULK1 complex. *Autophagy* **2018,** *14* (7), 1201-1213.
79. *Roczniak-Ferguson A., Petit C.S., Froehlich F., Qian S., Ky J., Angarola B., Walther T.C., Ferguson S.M.,* **T**he Transcription Factor TFEB Links mTORC1 Signaling to Transcriptional Control of Lysosome Homeostasis**.** *Sci Signal. 2012 Jun 12;5(228):ra42.*
80. Calderon BM, Danzy S, Delima GK, Jacobs NT, Ganti K, et al. Dysregulation of M segment gene expression contributes to influenza A virus host restriction. PLOS Path. 2019, 15(8): e1007892.
81. Zhang J, Ruan T, Sheng T, Wang J, Sun J, Wang J, Prinz RA, Peng D, Liu X, Xu X. Role of c-Jun terminal kinase (JNK) activation in influenza A virus-induced autophagy and replication. Virology. 2019 Jan 2; 526:1-12.
82. Martin KR, Celano SL, Solitro AR, Gunaydin H, Scott M, O'Hagan RC, Shumway SD, Fuller P, MacKeigan JP. A Potent and Selective ULK1 Inhibitor Suppresses Autophagy and Sensitizes Cancer Cells to Nutrient Stress. iScience. 2018 Oct 26;8:74-84.
83. Egan DF, Chun MG, Vamos M, Zou H, Rong J, Miller CJ, Lou HJ, Raveendra-Panickar D, Yang CC, Sheffler DJ, Teriete P, Asara JM, Turk BE, Cosford ND, Shaw RJ. Small Molecule Inhibition of the Autophagy Kinase ULK1 and Identification of ULK1 Substrates. Mol Cell. 2015 Jul 16;59(2):285-97.
84. Liu S, Xu SW, Kennedy L, Pala D, Chen Y, Eastwood M, Carter DE, Black CM, Abraham DJ, Leask A. FAK is required for TGFbeta-induced JNK phosphorylation in fibroblasts: implications for acquisition of a matrix-remodeling phenotype. Mol Biol Cell. 2007 Jun;18(6):2169-78.

FIGURE LEGENDS

Figure 1. The activation dynamics of genes involved in autophagy regulation are determined by IAV titer. Accumulation of viral transcripts (**A**) and autophagy regulating gene transcripts (**B**) in A549 cells at early (1-3 hpi), mid (6-8 hpi), and late stage (12 hpi) of the viral replication cycle at two multiplicities of infection (MOI) as determined by RNA-seq analysis (FDR-corrected $p < 0.01$). (**B**) Dendrograms of the hierarchical clustering of DGE show significant

difference in gene expression dynamics at the two MOIs. (**C**) Schematic of the autophagy pathway showing key regulatory proteins involved in each step of autophagosome formation.

Figure 2. Transcriptional activation of mTORC and ULK1 pathways in IAV-infected A549 cells. Gene activation dynamics were determined in A549 cells infected with IAV *P/Ch/1/73* at MOI1 and MOI5 versus mock treated cells at 1, 3, 4, 6, 8, and 12 hpi. Fold change differences of gene expression levels in IAV-infected relative to mock-treated cells are statistically significant between the two groups (FDR-corrected $p < 0.01$).

Figure 3. Activation of autophagy in IAV *P/Ch/1/73* infected A549 cells is not dependent on ULK-S757 phosphorylation by mTORC1. (**A**) Western blot analysis was performed on total protein isolated from IAV-infected (+) and mock-treated (-) A549 cells at mid (6 hpi) and later stage (7-8 hpi) of virus replication cycle. The ratio between lipidated (LC3B-II) and unprocessed (LC3B-I) forms of MAP1LC3B protein was used to determine the autophagy activation event. The activation status of mTOR and ULK1 proteins was determined as ratio between the mTOR-S2448 and ULK1-S757 phosphorylated versus respective total proteins. Untreated and SBI0206965 [10 μM] treated A549 cells were infected with IAV *P/Ch/1/73* at MOI5 and total protein was collected at the indicated hours post infection (hpi) together with the time-matched mock treated samples. Accumulation of the viral nucleoprotein (NP) and matrix 2 (M2) protein was analyzed relative to beta-Actin protein levels. (**B**) Quantitative analysis of protein band densities was performed on five independent experiments with Image Lab 6.0 (BioRad). Shown are the mean and standard deviations. (**C**) Fluorescent microscopy of A549 cells mock-treated or infected with IAV *P/Ch/1/73* at MOI5. A549 cells treated with the ULK inhibitor, SBI0206965 [10 μM], were equally infected and processed. Cells were fixed 8 hpi and were treated with primary antibodies against LC3B protein (red) and IAV matrix 2 (green). The cell nuclei were stained with DAPI (blue). The yellow arrows indicate at autophagosome formations. The white

scale bar corresponds to 10 μm. Shown is a representative of 3 independent biological replicas of IAV infected A549 cells.

Figure 4. Phosphorylation of SAPK/JNK-Thr183/Tyr185 coincides with AKT-pSer473 anti-apoptotic signaling and is essential for viral protein accumulation in IAV *P/Ch/1/73* infected A549 cells. (**A**) The mTORC1 and mTORC2 activity was deduced from the phosphorylation status of their corresponding substrates, p70S6K-Thr389 and AKT-S473, in IAV-infected (MOI1) cells. (**B**) mTORC1 activity was measured at later stage of IAV infection (6 and 8 hpi) at MOI 1, 5, and 10. (**C**) Western blot analysis of phosphorylated JNK-Thr183/Tyr185, total JNK, and IAV nucleocapsid protein (IAV-NP) in samples isolated from virus-infected (V) A549 cells at MOI5 and mock-treated (M) cells. JNK signaling was consequently activated with accumulation of viral protein at mid-to-late stage of the virus replication cycle. (**D**) Western blot analysis shows that chemical inhibition of SAPK/JNK signaling with SP600125 [10 μM] resulted in inhibition of virus protein (IAV-M2) accumulation in A549 cells. In the same samples, increase in the LC3B-II/LC3B-I ratio indicate that high viral protein levels are responsible for the SAPK/JNK and autophagy activation. Shown is a representative of four independent virus infection (MOI5) experiments.

Figure 5. Non-cancer lung bronchial epithelial cells exhibit higher dependence on JNK signaling for production of infectious IAV particles. (**A**) Chemical inhibition of ULK (SBI0206965 [1 μM]) and JNK (SP600125 [5 μM]) signaling showed divergent effects on the production of viral protein and LC3B in normal human bronchial epithelial cells (NHBE). Shown is a representative of three independent Western blot experiments of later stage (24 hpi) IAV infection at MOI5. (**B**) Immunofluorescence with antibodies targeting LC3B and IAV protein M2 demonstrated the effect of JNK-phT183 inhibition on the reduction of virus-

infected NHBEC. Images were acquired 24 hpi at MOI5. The white scale bar corresponds to 60 µm. The graph presents the percent of cells harboring viral M2 protein. Image quantification of IAV-M2-labeled cells was performed on > 300 cells in random fields for four independent infection experiments. (**C**) Inhibition of virus protein synthesis was consistent with reduction of infectious virus load, measured as plaque forming units per mL conditioned media (PFU/mL), generated by A549, BEAS-2B, and NHBE treated with inhibitors of ULK or JNK signaling compared to the not treated (NT) controls. The PFU/mL were determined 40 hpi with IAV-*A/PCh/1/73* at MOI5. The statistical significance of the results was determined from four independent infection experiments with Student t-test (* $p < 0.01$ and ** $p < 0.001$).

Figure 6. IAV-M2 recruits LC3B in the cell membranes. Fluorescent microscopy of HEK293T cells transfected with plasmids expressing G10- and G11-tagged IAV-M2 and LC3B proteins demonstrate that direct interaction between the two proteins occur on the cell plasma membrane or intracellular membranous vesicles. Shown are images of split-GFP complementation assay 48 hours after transfection of HE293T cells with the corresponding plasmids. The GFP1-9 scaffold was supplied as purified and folded protein in fixed and permeabilized cells.

Supplementary Materials:

Figure S1: Microscopic analysis of TFEB cellular localization in serum sufficient and serum starved A549 cells infected with IAV *A/Port Chalmers/1/73* (H3N2) at MOI1. Time laps microscopy of A549 cell line with stable expression of TFEB fused to GFP demonstrated that the autophagy regulating transcription factor localized within the cell nucleus within 40 min of serum

978 starvation during the virus absorption phase in both virus infected and MOCK-treated cells (A).
979 The scale bar equals 10μm. The phosphorylated levels of mTORC1 substrate, ribosomal protein
980 p70S6K1, sharply decreased in both IAV infected and MOCK-treated cells during the virus
981 absorption phase in serum-depleted media (B). ELISA data from three independent infection
982 experiments presents the ratio between sample absorbance at each indicated time point relative to
983 time-0 sample absorbance. The replication efficiencies of H3N2 and H1N1 (*A/Puerto Rico/8/34*)
984 IAV subtypes varied significantly in A549 cell line (D) as measured by plaque forming units assay
985 (PFU). Shown are the results from three independent infection experiments at MOI 5. Time-lapse
986 microscopy of A549 cell line with stable expression of TFEB-GFP showed accumulation of the
987 autophagy master regulator in the cell nucleus on the second hour of infection that followed the 1h
988 (60") virus absorption phase (E) in serum replete medium. The scale bar equals 10μm.

989 **Figure S2**: Schematic presentation of mTORC signaling pathways with differential activation
990 patterns of key regulatory genes at 1 and 5 MOI of IAV *A/Port Chalmers/1/73* (H3N2)

991 **Figure S3**: (A) Western blot (WB) analysis of IAV protein accumulation, NP and M2, and (B)
992 flow cytometry analysis of infected A549 cells at two different MOIs demonstrate the limitations
993 of WB sensitivity when protein accumulation dynamics are studied. (C) Western Blot analysis of
994 phosphorylated Thr183-JNK accumulation in A549 cells infected with the IAV H1N1 subtype
995 (MOI 5) reveals correlation between host cell permissiveness to virus replication and activation of
996 JNK signaling. Shown is a representative of three independent virus infection experiments.

997

998 **Table S1**: Sequences of viral (M2) and host (LC3B) proteins tagged with GFP fragments for tri-
999 party complementation assay *in situ*.

GFP11-M2	MEKRDHMVLLEYVTAAGITDASGTDVGSGGGSGGGGSGGSSLLTEVE TPIRNEWGCRCNDSSDPLVVAASIIGILHLILWILDRLFFKCIYRFFEHGL KRGPSTEGVPESMREEYRKEQQSAVDADDSHFVSIELE*
M2 –GFP11	MSLLTEVETPIRNEWGCRCNDSSDPLVVAASIIGILHLILWILDRLFFKCI YRFFEHGLKRGPSTEGVPESMREEYRKEQQSAVDADDSHFVSIELEGGS GSGGGGSGGGSGGGSTSEKRDHMVLLEYVTAAGITDAS*
GFP10-M2	MDLPDDHYLSTQTILSKDLNGTDVGSGGGSGGGGSGGSSLLTEVETPIR NEWGCRCNDSSDPLVVAASIIGILHLILWILDRLFFKCIYRFFEHGLKRGP STEGVPESMREEYRKEQQSAVDADDSHFVSIELE*
M2-GFP10	MSLLTEVETPIRNEWGCRCNDSSDPLVVAASIIGILHLILWILDRLFFKCI YRFFEHGLKRGPSTEGVPESMREEYRKEQQSAVDADDSHFVSIELEGGS GSGGGGSGGGSGGGSTSDLPDDHYLSTQTILSKDLN*
GFP10 – LC3B	MDLPDDHYLSTQTILSKDLNGTDVGSGGGSGGGGSGGSMPSEKTFKQR RTFEQRVEDVRLIREQHPTKIPVIIERYKGEKQLPVLDKTKFLVPDHVN MSELIKIIRRRLQLNANQAFFLLVNGHSMVSVSTPISEVYESEKDEDGFL YMVYASQETFGMKLSV*
LC3B-GFP10	MPSEKTFKQRRTFEQRVEDVRLIREQHPTKIPVIIERYKGEKQLPVLDKT KFLVPDHVNMSELIKIIRRRLQLNANQAFFLLVNGHSMVSVSTPISEVYE SEKDEDGFLYMVYASQETFGMKLSVGGSGSGGGGSGGGSGGGSTSDL PDDHYLSTQTILSKDLN*

1003

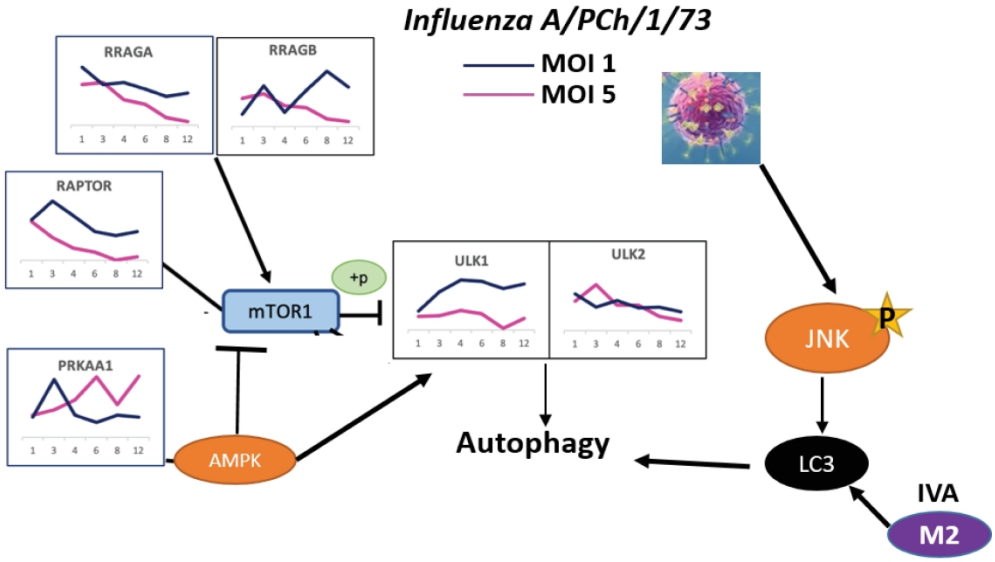

Genes regulating mTORC1 and ULK1 pathways are simultaneously activated in Influenza A infected lung cells. The activation profile of mTORC1 and autophagy regulating genes is influenced by the viral load. Stress-activated protein kinase (SAPK/JNK) signaling is triggered by high viral protein load and coincides with activation of autophagy.

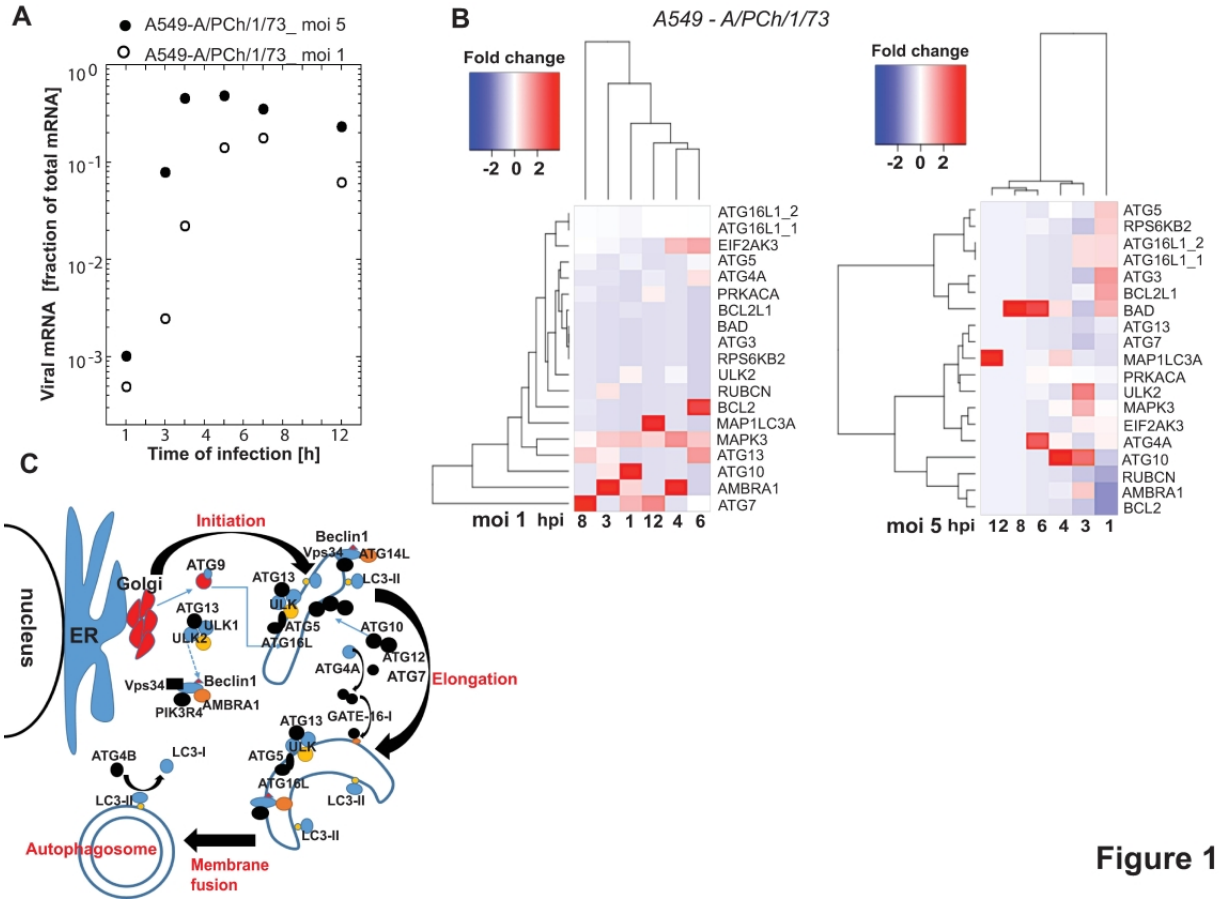

Figure 1

Figure 1. IAV load strongly influenced the activation dynamics of genes involved in autophagy regulation. Accumulation of viral transcripts (A) and autophagy regulating gene transcripts (B) in A549 cells at early (1-3 hpi), mid (6-8 hpi), and late stage (12 hpi) of the viral replication cycle at two multiplicities of infection (MOI) as determined by RNA-seq analysis (FDR-corrected $p < 0.01$). Dendrograms of the hierarchical clustering of DEG (B) show significant difference in gene expression dynamics at the two MOIs. Schematic of the autophagy pathway (C) showing key regulatory proteins involved in each step of autophagosome formation.

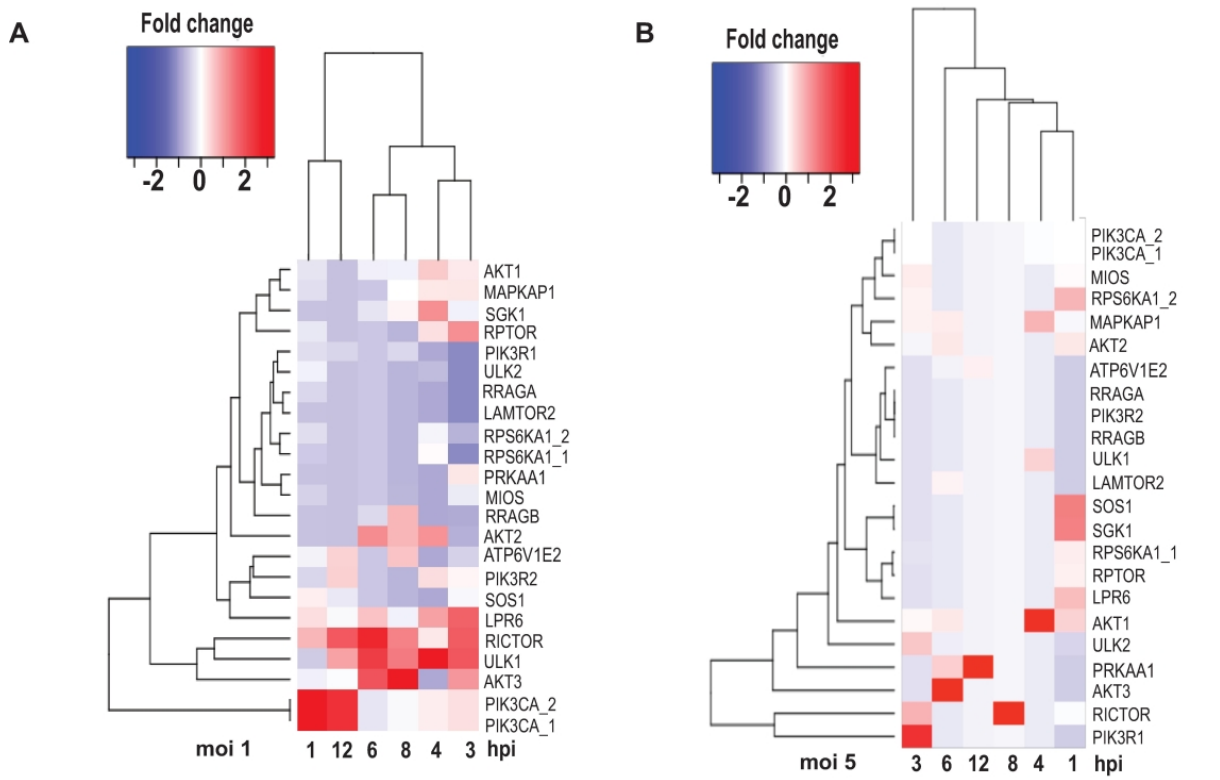

Figure 2

Figure 2. Transcriptional activation of mTORC and ULK1 pathways in IAV-infected A549 cells. Gene activation dynamics were determined in A549 cells infected with IAV P/Ch/1/73 at MOI1 and MOI5 versus mock treated cells at 1, 3, 4, 6, 8, and 12 hpi. Fold change differences of gene expression levels in IAV-infected relative to mock-treated cells are statistically significant between the two groups (FDR-corrected $p < 0.01$).

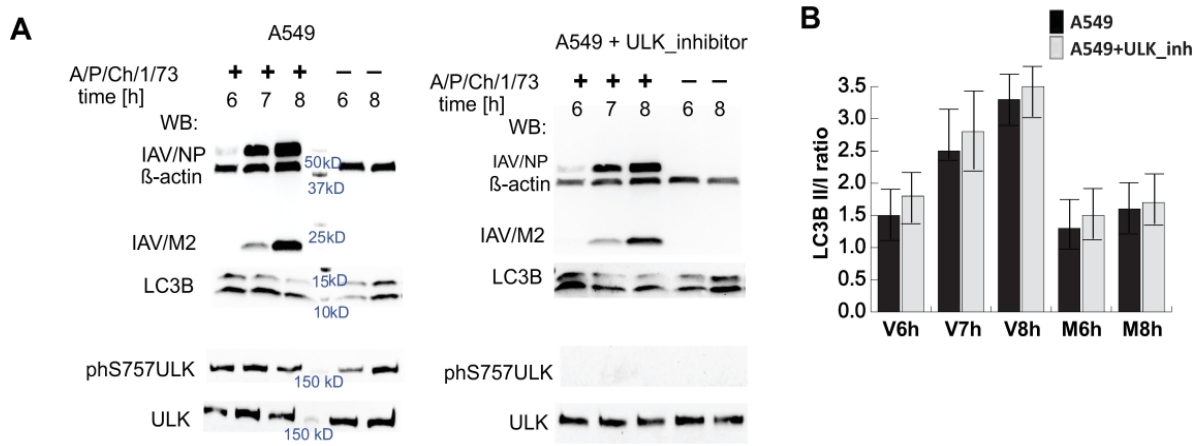

Figure 3

Figure 3. Activation of autophagy in IAV P/Ch/1/73 infected A549 cells is not dependent on ULK-S757 phosphorylation by mTORC1. (A) Western blot analysis was performed on total protein isolated from IAV-infected (+) and mock-treated (-) A549 cells at mid (6 hpi) and later stage (7-8 hpi) of virus replication cycle. The ratio between lipidated (LC3B-II) and unprocessed (LC3B-I) forms of MAP1LC3B protein was used to determine the autophagy activation event. The activation status of mTOR and ULK1 proteins was determined as ratio between the mTOR-S2448 and ULK1-S757 phosphorylated versus respective total proteins. Untreated and SBI0206965 [10 □M] treated A549 cells were infected with IAV P/Ch/1/73 at MOI5 and total protein was collected at the indicated hours post infection (hpi) together with the time-matched mock treated samples. Accumulation of the viral nucleoprotein (NP) and matrix 2 (M2) protein was analyzed relative to beta-Actin protein levels. (B) Quantitative analysis of protein band densities was performed on five independent experiments with Image Lab 6.0 (BioRad). Shown are the mean and standard deviations.

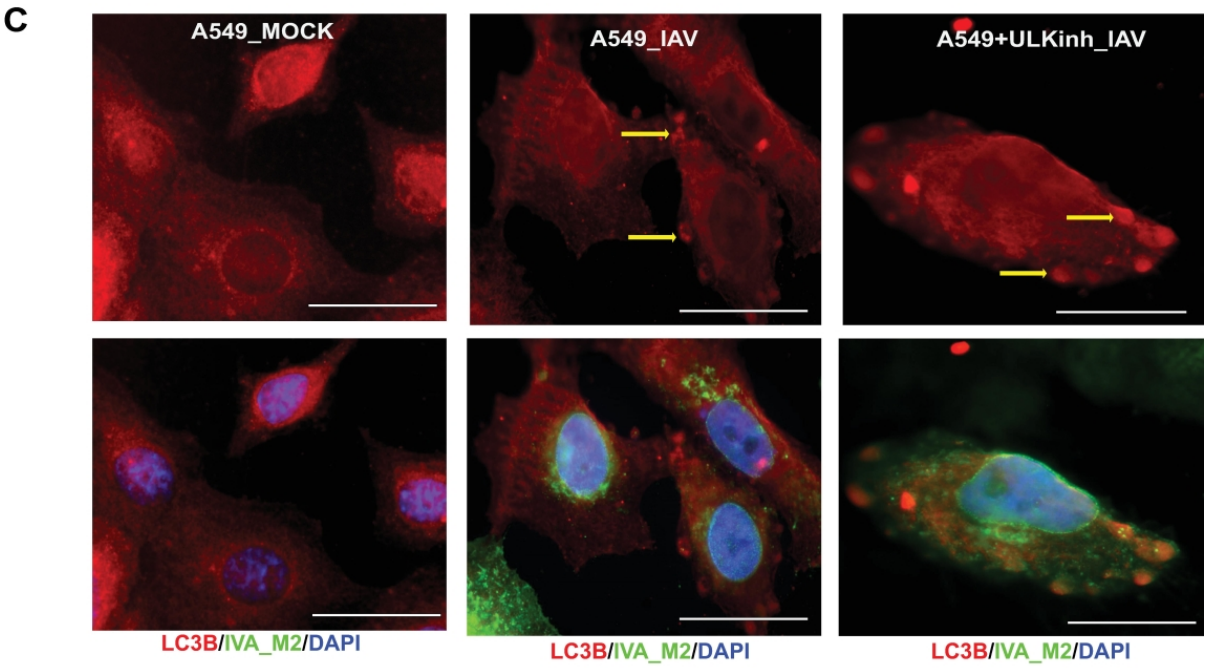

Figure 3

Fig. 3 (C) Fluorescent microscopy of A549 cells mock-treated or infected with IAV P/Ch/1/73 at MOI5. A549 cells treated with the ULK inhibitor, SBI0206965 [10 ,]M were equally infected and processed. Cells were fixed 8 hpi and were treated with primary antibodies against LC3B protein (red) and IAV matrix 2 (green). The cell nuclei were stained with DAPI (blue). The yellow arrows indicate at autophagosome formations. The white scale bar corresponds to 10 μm. Shown is a representative of 3 independent biological replicas of IAV infected A549 cells.

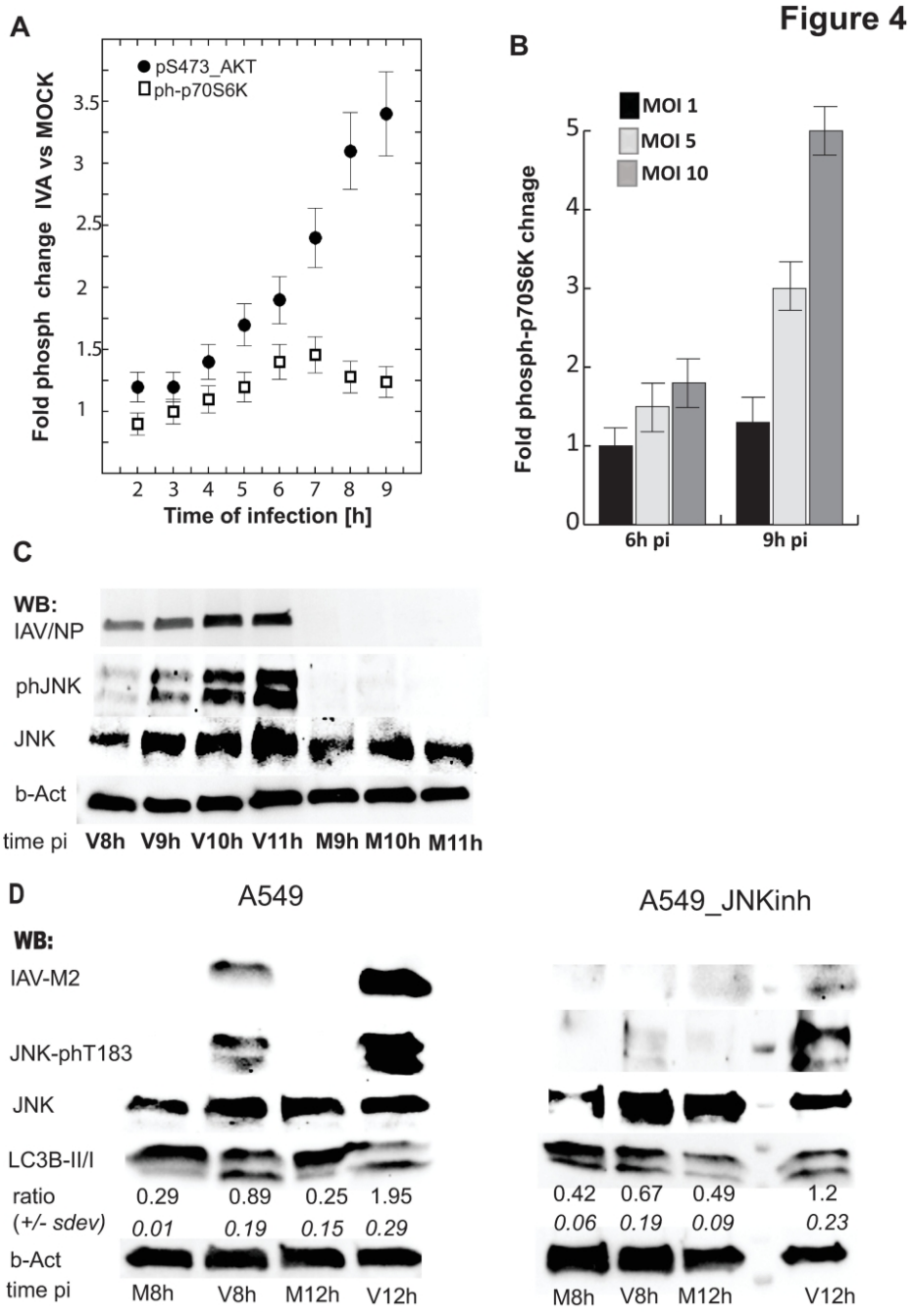

Figure 4. Phosphorylation of SAPK/JNK-Thr183/Tyr185 coincides with AKT-pSer473 anti-apoptotic signaling and is essential for viral protein accumulation in IAV P/Ch/1/73 infected A549 cells. (A) The mTORC1 and mTORC2 activity was deduced from the phosphorylation status of their corresponding substrates, p70S6K-Thr389 and AKT-S473, in IAV-infected (MOI1) cells. (B) mTORC1 activity was measured at later stage of IAV infection (6 and 8 hpi) at MOI 1, 5, and 10. (C) Western blot analysis of phosphorylated JNK-Thr183/Tyr185, total JNK, and IAV nucleocapsid protein (IAV-NP) in samples isolated from virus-infected (V) A549 cells at MOI5 and mock-treated (M) cells. JNK signaling was consequently activated with accumulation of viral protein at mid-to-late stage of the virus replication cycle. (D) Western blot analysis shows that chemical inhibition of SAPK/JNK signaling with SP600125 [10]M resulted in inhibition of virus protein (IAV-M2) accumulation in A549 cells. In the same samples, increase in the LC3B-II/LC3B-I ratio indicate that high viral protein levels are responsible for the SAPK/JNK and autophagy activation. Shown is a representative of four independent virus infection (MOI5) experiments.

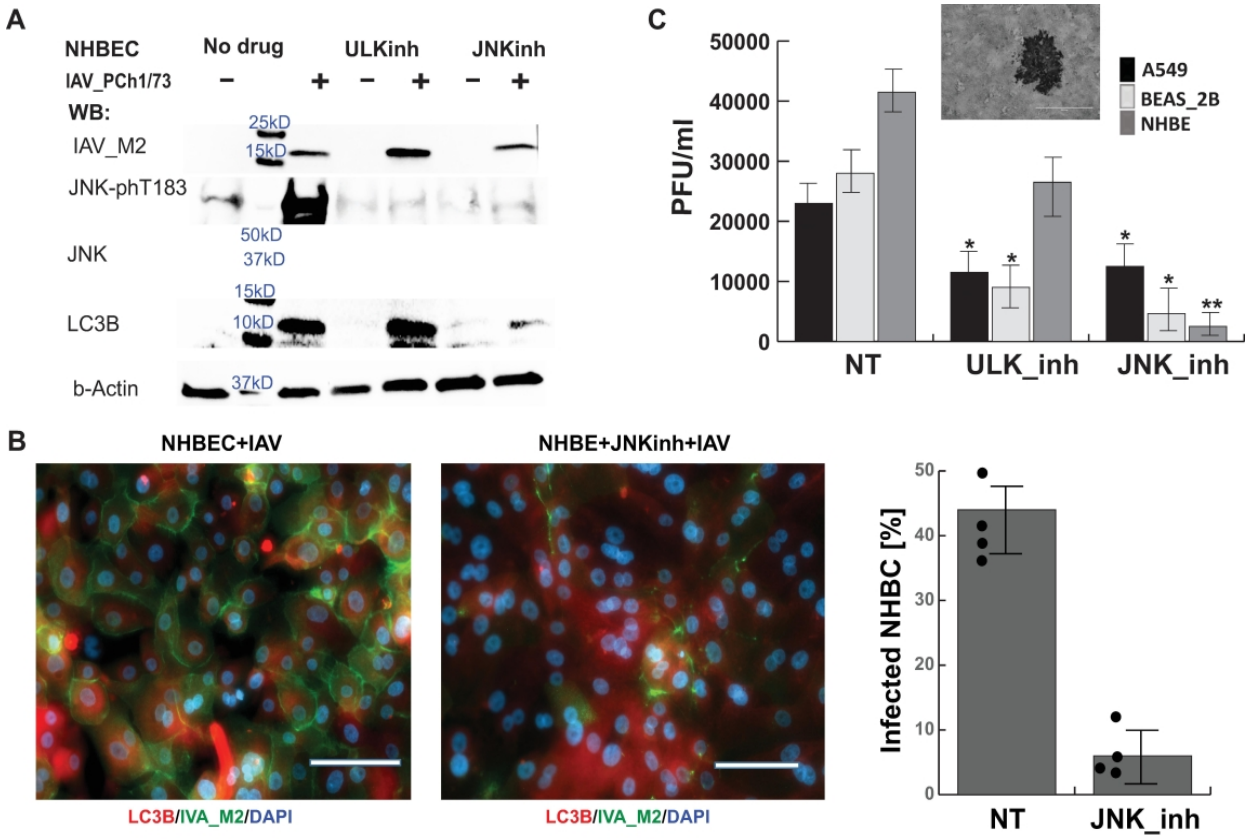

Figure 5. Non-cancer lung bronchial epithelial cells exhibit higher dependence on JNK signaling for production of infectious IAV particles. (A) Chemical inhibition of ULK (SBI0206965 [1 ☐M]) and JNK (SP600125 [5 ☐M]) signaling showed divergent effects on the production of viral protein and LC3B in normal human bronchial epithelial cells (NHBE). Shown is a representative of three independent Western blot experiments of later stage (24 hpi) IAV infection at MOI5. (B) Immunofluorescence with antibodies targeting LC3B and IAV protein M2 demonstrated the effect of JNK-phT183 inhibition on the reduction of virus-infected NHBEC. Images were acquired 24 hpi at MOI5. The white scale bar corresponds to 60 μm. The graph presents the percent of cells harboring viral M2 protein. Image quantification of IAV-M2-labeled cells was performed on > 300 cells in random fields for four independent infection experiments. (C) Inhibition of virus protein synthesis was consistent with reduction of infectious virus load, measured as plaque forming units per mL conditioned media (PFU/mL), generated by A549, BEAS-2B, and NHBE treated with inhibitors of ULK or JNK signaling compared to the not treated (NT) controls. The PFU/mL were determined 40 hpi with IAV-A/PCh/1/73 at MOI5. The statistical significance of the results was determined from four independent infection experiments with Student t-test (* $p < 0.01$ and ** $p < 0.001$).

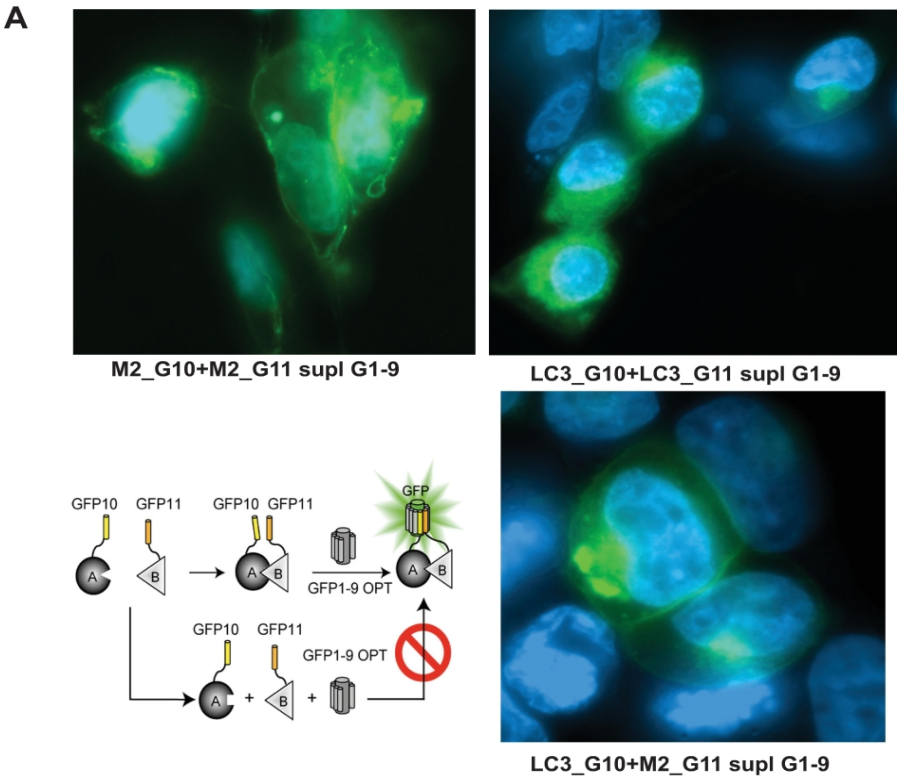

Figure 6

Figure 6. IAV-M2 recruits LC3B in the cell membranes. Fluorescent microscopy of HEK293T cells transfected with plasmids expressing G10- and G11-tagged IAV-M2 and LC3B proteins demonstrate that direct interaction between the two proteins occur on the cell plasma membrane or intracellular membranous vesicles. Shown are images of split-GFP complementation assay 48 hours after transfection of HE293T cells with the corresponding plasmids. The GFP1-9 scaffold was supplied as purified and folded protein in fixed and permeabilized cells.

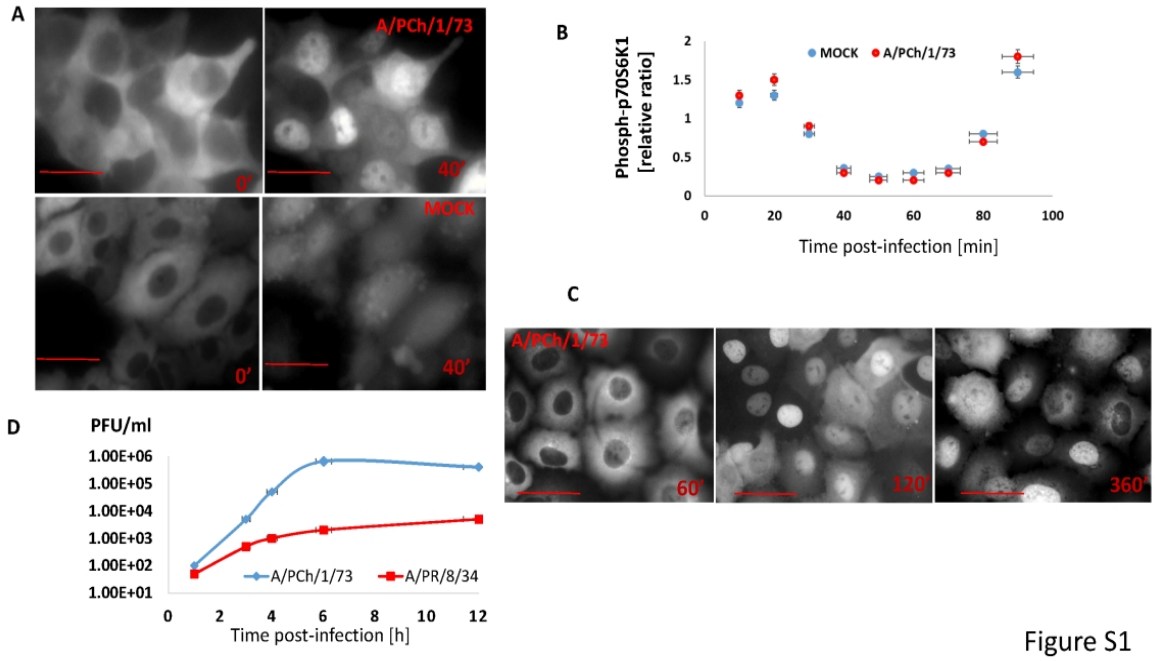

Figure S1

Figure S1: Microscopic analysis of TFEB cellular localization in serum sufficient and serum starved A549 cells infected with IAV A/Port Chalmers/1/73 (H3N2) at MOI1. Time laps microscopy of A549 cell line with stable expression of TFEB fused to GFP demonstrated that the autophagy regulating transcription factor localized within the cell nucleus within 40 min of serum starvation during the virus absorption phase in both virus infected and MOCK-treated cells (A). The scale bar equals 10μm. The phosphorylated levels of mTORC1 substrate, ribosomal protein p70S6K1, sharply decreased in both IAV infected and MOCK-treated cells during the virus absorption phase in serum-depleted media (B). ELISA data from three independent infection experiments presents the ratio between sample absorbance at each indicated time point relative to time-0 sample absorbance. The replication efficiencies of H3N2 and H1N1 (A/Puerto Rico/8/34) IAV subtypes varied significantly in A549 cell line (D) as measured by plaque forming units assay (PFU). Shown are the results from three independent infection experiments at MOI 5. Time-lapse microscopy of A549 cell line with stable expression of TFEB-GFP showed accumulation of the autophagy master regulator in the cell nucleus on the second hour of infection that followed the 1h (60") virus absorption phase (E) in serum replete medium. The scale bar equals 10μm.

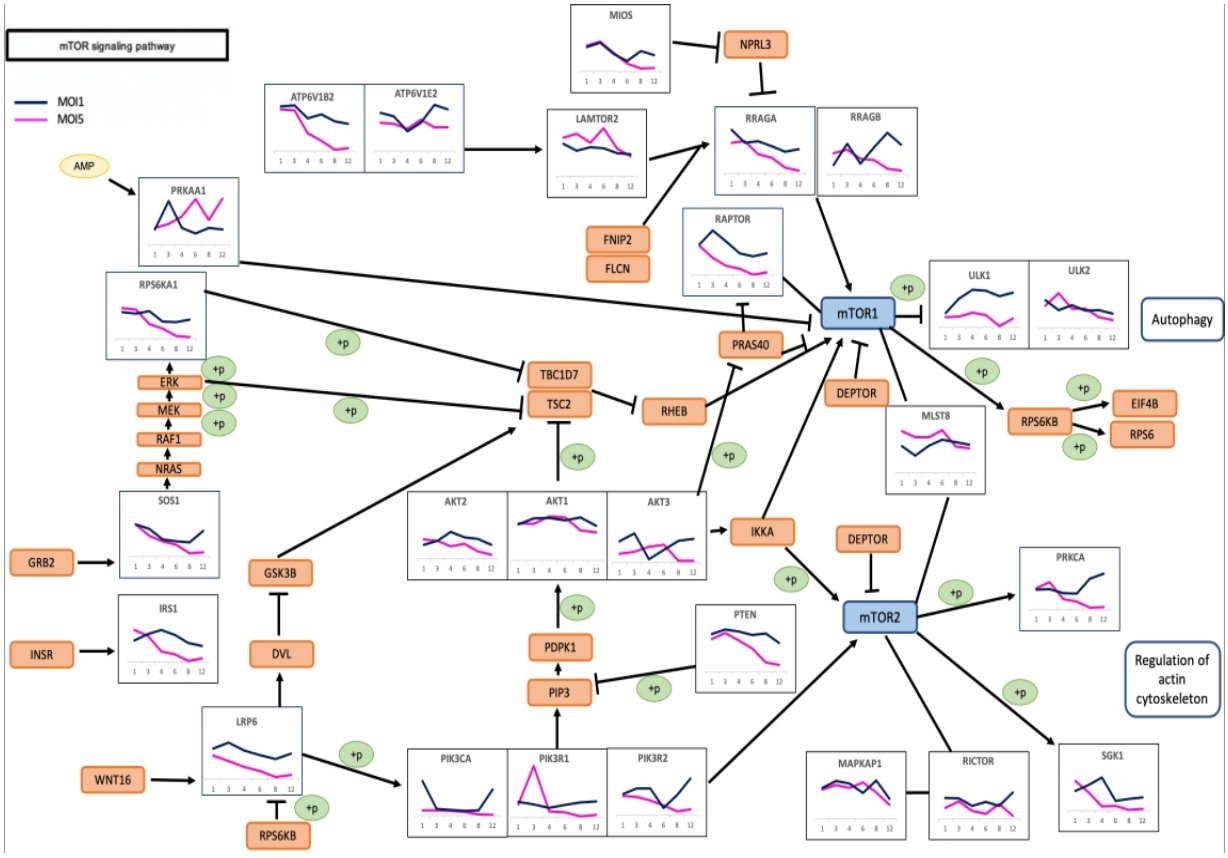

Figure S2: Schematic presentation of mTORC signaling pathways with differential activation patterns of key regulatory genes at 1 and 5 MOI of IAV A/Port Chalmers/1/73 (H3N2)

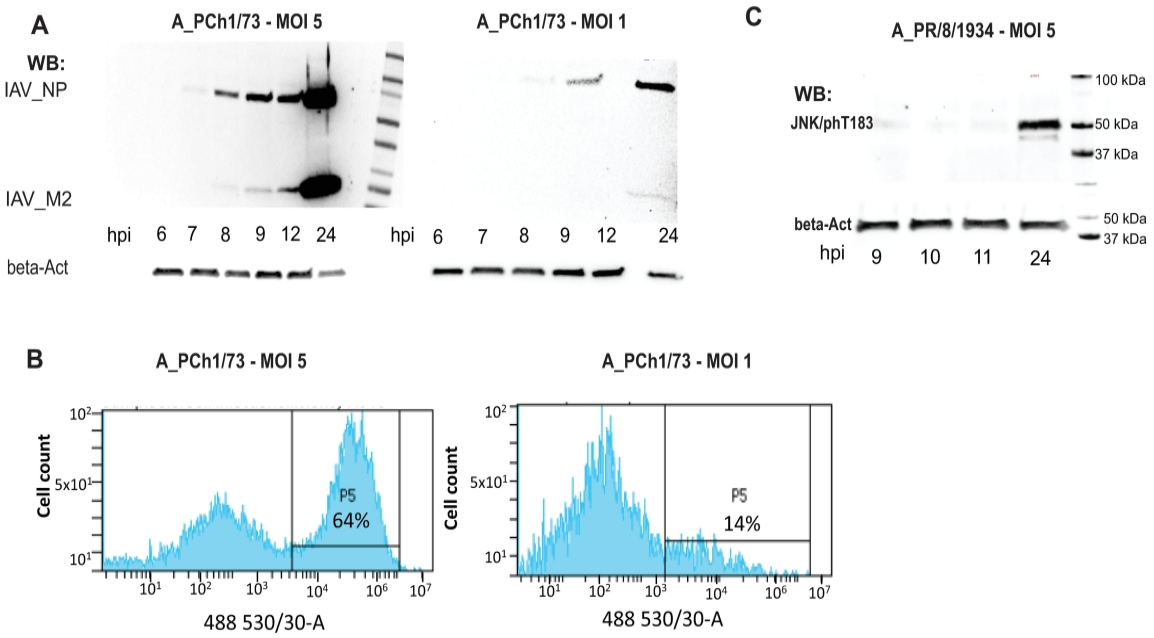

Figure S3: (A) Western blot (WB) analysis of IAV protein accumulation, NP and M2, and (B) flow cytometry analysis of infected A549 cells at two different MOIs demonstrate the limitations of WB sensitivity when protein accumulation dynamics are studied. (C) Western Blot analysis of phosphorylated Thr183-JNK accumulation in A549 cells infected with the IAV H1N1 subtype (MOI 5) reveals correlation between host cell permissiveness to virus replication and activation of JNK signaling. Shown is a representative of three independent virus infection experiments.